Editors' Suggestion | Featured in Physics

nnn and *ppp* correlation functions

A. Kievsky [1], E. Garrido [2], M. Viviani [1], L. E. Marcucci [3,1], L. Šerkšnytė [4], and R. Del Grande [4,5]

[1] *Istituto Nazionale di Fisica Nucleare, Largo Pontecorvo 3, 56127 Pisa, Italy*
[2] *Instituto de Estructura de la Materia, IEM-CSIC, Serrano 123, E-28006 Madrid, Spain*
[3] *Physics Department, University of Pisa, Largo Pontecorvo 3, 56127 Pisa, Italy*
[4] *Physik Department E62, Technische Universität München, James-Franck-Straße 1, 85748 Garching, Germany*
[5] *Excellence Cluster ORIGINS, Boltzmannstraße 2, 85748 Garching, Germany*

(Received 18 October 2023; revised 15 January 2024; accepted 29 January 2024; published 29 March 2024)

Scattering experiments with three free nucleons in the ingoing channel are extremely challenging in terrestrial laboratories. Recently, the ALICE Collaboration successfully measured the scattering of three protons indirectly, by using the femtoscopy method in high-energy proton-proton collisions at the Large Hadron Collider. In order to establish a connection with current and future measurements of femtoscopic three-particle correlation functions, we analyze the scenarios involving *nnn* and *ppp* systems using the hyperspherical adiabatic basis. The correlation function is a convolution of the source function and the corresponding scattering wave function. The finite size of the source allows for the use of the free scattering wave function in most of the adiabatic channels except the lowest ones. The scattering wave function has been computed using two different potential models: (*i*) a spin-dependent Gaussian potential with parameters fixed to reproduce the scattering length and effective range and (*ii*) the Argonne v_{18} nucleon-nucleon interaction. Moreover, in the case of three protons, the Coulomb interaction has been considered in its hypercentral form. The results presented here have to be considered as a first step in the description of three-particle correlation functions using the hyperspherical adiabatic basis, opening the door to the investigation of other systems, such as the $pp\Lambda$ system. For completeness, the comparison with the measurement by the ALICE Collaboration is shown assuming different values of the source radius.

DOI: 10.1103/PhysRevC.109.034006

I. INTRODUCTION

In the past few years, the femtoscopy technique [1–3] has been applied in high-energy *pp* and *p*-Pb collisions at the Large Hadron Collider (LHC) to study the residual strong interaction between hadrons [4]. In such collisions, particles are produced and emitted at relative distances of the order of a femtometer, in the range of the nuclear force. The effect of the mutual interaction between hadrons is reflected as a correlation signal in the momentum distributions of the detected particles which can be studied using correlation functions. The latter incorporate information on the emission process as well as on the final state interaction of the emitted pairs at the femtoscopic scale. Therefore, by measuring correlated particle pairs at low relative energies and comparing the yields to theoretical predictions, it is possible to perform a new study of the hadron dynamics. The high precision measurements obtained by the ALICE Collaboration in the strangeness sector made it possible to test lattice calculations for the first time and to challenge effective field theory results (for a comprehensive review see [4] and references therein).

The next challenge is to extend the method to test the hadronic interactions in three-body systems. Recently, the *ppp* and *pd* correlation functions were measured by the ALICE Collaboration [5,6]. The interpretation of the former measurement requires a correct treatment of the three-proton scattering wave function which has to be used as input in the computation of the corresponding correlation function. This observable reflects a complex structure mainly determined when the three hadrons have low relative momenta. Traditional low-energy scattering experiments with three free hadrons in the ingoing channel are currently not yet available. Therefore the femtoscopic measurement gives a unique opportunity to study a $3 \to 3$ scattering process. In the *pd* case a very detailed discussion was recently performed [7], showing that the description of the data is possible when a very sophisticated *pd* scattering wave function is used.

In the present work, we would like to set the basis for the study of the three-particle correlation function. Specifically, we will focus on the *ppp* correlation function, whose description presents intrinsic difficulties due to the long-range Coulomb interaction. The asymptotic description of three charged particles has always attracted a lot of attention since it is present in many different systems: atomic, nuclear, and subnuclear systems (for a recent discussion see Ref. [8]). In this preliminary study, we perform a simplification in the asymptotic description of the three protons and concentrate on the different steps needed in the computation of the *ppp* correlation function. However, at the end of the study we give indications of the corrections due to a complete treatment of the Coulomb interaction.

We would like to stress that the present study represents the first step in the description of the three-particle correlation functions and will serve as a guideline for future studies of systems including hyperons such as the $pp\Lambda$ system.

The paper is organized as follows: after introducing the main ingredients of the method and the correlation function, we briefly present the two-body case needed to define the notation and the procedure. The results are compared to previous calculations and the data published by the ALICE Collaboration [9]. Then we describe the three-body case: first the *nnn* and then the *ppp* system. In all cases, we discuss how to construct the free asymptotic wave function with the proper symmetry. In fact, more and more partial waves are needed to correctly describe the correlation function when increasing the energy. The calculated *ppp* correlation function is finally compared to measurements by the ALICE Collaboration in *pp* collisions at center-of-mass energy 13 TeV at the LHC. The last section is devoted to the conclusions.

II. CORRELATION FUNCTION

In order to compute the *ppp* correlation function, two main ingredients are needed: the source function and the *ppp* wave function at different energies. The former is modelled as the product of three single Gaussian emitters, depending only on the size of the source. For the latter, we use the hyperspherical harmonic (HH) method [10,11] in conjunction with the adiabatic harmonic (HA) basis [12]. These two methods have been extensively used in the description of the three-nucleon continuum [13–17].

In the present case, we apply these methods to describe the *ppp* system. Essentially we decompose the *ppp* wave function in partial waves having well-defined values of total angular momentum and parity, J^π. After introducing the hyperspherical coordinates we solve the hyperangular Hamiltonian including the different partial waves compatible with the lowest values of the grand angular quantum number K. Here we show that the lowest adiabatic channel provides sufficient accuracy. We pay particular attention to the construction of the different spatial and spin symmetries entering in the description of the wave function. We discuss these elements first in the *nnn* case, where the Coulomb interaction is not present. Then we extend the analysis to the *ppp* case considering the Coulomb interaction in the hypercentral approximation. In this way, the asymptotic wave function can be evaluated analytically. It will be shown that the structure of the *ppp* and the *nnn* correlation functions are mostly determined by the lowest partial waves in which the nuclear interaction appreciably distorts the free scattering wave function.

Regarding the *pp* or *nn* interactions, taking advantage of the fact that the *pp* and *nn* systems are located inside the universal window [18], we first use a Gaussian potential model constructed to reproduce the corresponding scattering lengths and effective ranges. This potential acts only in s wave. Then we incorporate in the study the results obtained using a more realistic potential, the Argonne v_{18} potential (AV18) [19] already used in earlier studies of the *pp* correlation function. At the end, we will estimate three-nucleon interaction effects using the AV18 potential in conjunction with the Urbana IX three-nucleon force [20].

First, the two-body case will be presented. The study of the two-particle scattering through the measurement of their correlation function is based on the femtoscopy method [1,3]. This method is used in high-energy collisions and measures correlated pairs of particles having low values of relative momentum. It was recently applied to measure hadron-hadron correlation functions such as *pp* [21], $pK^\pm$ [22,23], $p\Lambda$ [24], $p\Sigma^0$ [9], $\Lambda\Lambda$ [25], $p\Xi^-$ [26], $\Lambda K^\pm$ [27] $p\Omega^-$ [28], $\Lambda\Xi$ [29], $p\phi$ [30] and baryon-antibaryon [31]. The final state interaction between measured particles was then studied by comparing the experimental values to the theoretical predictions.

For two-body systems, the correlation function is defined in terms of the relative momentum k between the particles in the pair rest frame by the Koonin-Pratt equation [32,33]

$$C_{12}(k) = \int d\boldsymbol{r}\, S_{12}(r)|\Psi_s|^2, \tag{1}$$

where $S_{12}(r)$ is the so-called source function, which is an effective parametrization of the properties of the particle emission process, defined in terms of the relative distances r between the particles, and $|\Psi_s|^2$ is the square of the scattering wave function of the two particles.

The correlation function can be generalized for a three-particle case as

$$C_{123}(Q) = \int \rho^5 d\rho\; d\Omega_\rho\, S_{123}(\rho)|\Psi_s|^2, \tag{2}$$

where $S_{123}(\rho)$ is a three-particle source function. Here, Q is the hypermomentum, ρ is the hyperradius, Ω_ρ corresponds to the set of five hyperangles, and $|\Psi_s|^2$ is the square of the scattering wave function of the three particles. The details of these variables are given in Sec. IV. While the two-particle scattering wave function has been already estimated for many different hadron-hadron and hadron-nucleus pairs, it has never been evaluated for the three-particle case, which is the goal of this work.

III. THE TWO-BODY CASE

As a preliminary step to analyze a three-particle scattering process, we discuss first the scattering wave function for two protons. Considering only the Coulomb interaction, the scattering wave function for two protons is

$$\Psi_s^0 = 4\pi \sum_{JJ_z} \sum_{\ell m S S_z} i^\ell \frac{F_\ell(\eta, kr)}{kr} \times (\ell m S S_z|JJ_z)\mathcal{Y}_{\ell S}^{JJ_z}(\Omega_r) Y_{\ell m}^*(\Omega_k), \tag{3}$$

where ℓ, S, and J are the relative orbital angular momentum, total spin, and total angular momentum, respectively, with projections m, S_z, and J_z; and Ω_r and Ω_k are the polar and azimuthal angles describing the directions of the relative coordinate ($\boldsymbol{r}$) and the relative momentum ($\boldsymbol{k}$).

In the expression above, $F_\ell(\eta, kr)$ is the regular Coulomb function with Sommerfeld parameter $\eta = e^2\mu/(\hbar^2 k)$, where μ is the reduced mass, and

$$\mathcal{Y}_{\ell S}^{JJ_z}(\Omega_r) = \sum_{m S_z} (\ell m\, S S_z|JJ_z) Y_{\ell m}(\Omega_r)\chi_{SS_z}, \tag{4}$$

where χ_{SS_z} is the spin function arising from the coupling of two spin-$\frac{1}{2}$ particles to $S = 0, 1$, and $Y_{\ell m}(\Omega_r)$ is a spherical harmonic function.

For two uncharged particles ($\eta = 0$), the Coulomb function, $F_\ell(\eta, kr)$, reduces to the Riccati-Bessel function $kr j_\ell(kr)$, and Eq. (3) becomes

$$\Psi_s^0 = e^{i\boldsymbol{k}\cdot\boldsymbol{r}} \sum_{SS_z} \chi_{SS_z}. \tag{5}$$

The expressions above are general, and valid for systems without any well-defined symmetry. However, for two identical nucleons the quantum numbers ℓ and S are restricted to those combinations allowed from the antisymmetry requirement. In this case ℓ and S are not independent, and we then introduce the index $[\ell S]$ indicating that $S = 0$ ($S = 1$) for even (odd) values of ℓ.

The norm of the scattering wave function, $|\Psi_s^0|^2_\Omega$, is defined as the average over the angular coordinates of the square of the wave function, i.e.,

$$\left|\Psi_s^0\right|^2_\Omega = \frac{1}{(4\pi)^2} \int d\Omega_r \int d\Omega_k \left|\Psi_s^0\right|^2, \tag{6}$$

which for the free case (no Coulomb), without any symmetry, and after introducing Eq. (5), becomes

$$\left|\Psi_s^0\right|^2_\Omega = N_S, \tag{7}$$

where $N_S = \sum_{SS_z} 1 = \sum_S (2S+1) = 4$ is the number of spin states.

In the case of antisymmetric wave functions some structure appears, and use of Eq.(3) leads to

$$\left|\Psi_s^0\right|^2_\Omega = \frac{2}{N_S} \sum_{[\ell S]} \left(\frac{F_\ell(\eta, kr)}{kr}\right)^2 N_{[\ell S]}, \tag{8}$$

where the factor of 2 is due to the fact that we are dealing with two identical particles, and where the $1/N_S$ factor—see Eq. (7)—has been introduced to impose $|\Psi_s^0|^2_\Omega \to 1$ as $r \to \infty$.

The quantity $N_{[\ell S]}$ is the number of allowed states. Without considering a particular symmetry the number of states would be $N_{[\ell S]} = 4(2\ell+1)$. However, for antisymmetric states we have that

$$N_{[\ell S]} = \begin{cases} (2\ell+1) & \text{if } \ell \text{ even}, \\ 3(2\ell+1) & \text{if } \ell \text{ odd}, \end{cases} \tag{9}$$

which leads to the following expression for the norm:

$$|\Psi_s^0|^2_\Omega = \frac{1}{2} \sum_{\ell \equiv \text{even}} \left(\frac{F_\ell(\eta, kr)}{kr}\right)^2 (2\ell+1) + \frac{3}{2} \sum_{\ell \equiv \text{odd}} \left(\frac{F_\ell(\eta, kr)}{kr}\right)^2 (2\ell+1). \tag{10}$$

In Fig. 1 the norm of the free scattering wave function, Eq. (10), is shown for the *nn* and *pp* systems, considering different values of η [for the *nn* case, $\eta = 0$ and $F_\ell(\eta, kr)$ has to be replaced by $kr j_\ell(kr)$]. The convergence has been achieved after the inclusion of ℓ values up to $\ell = 40$.

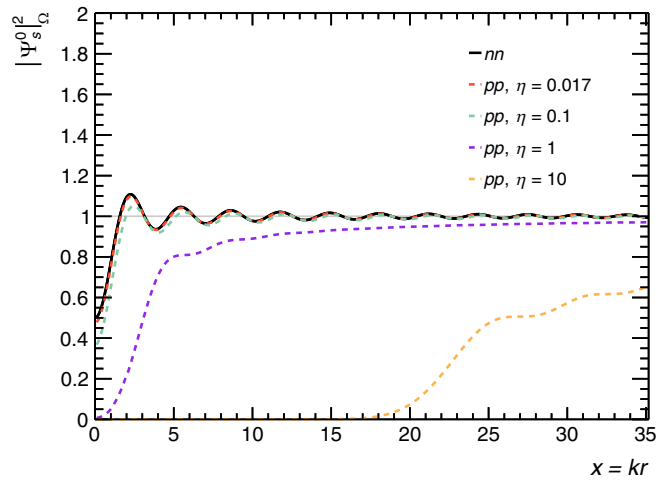

FIG. 1. The norm of the scattering wave function, Eq. (10), for the *nn* and *pp* cases. For the latter, different values of η have been considered.

A. Introducing the strong interaction

For convenience let us write Eq. (3) as

$$\Psi_s = 4\pi \sum_{JJ_z} \sum_{\ell m S S_z} i^\ell \Psi_{\ell S}^{JJ_z}(\ell m S S_z | JJ_z) Y^*_{\ell m}(\Omega_k), \tag{11}$$

where $\Psi_{\ell S}^{JJ_z} = (kr)^{-1} F_\ell(\eta, kr) \mathcal{Y}_{\ell S}^{JJ_z}(\Omega_r)$ is just the coordinate wave function of the system with quantum numbers ℓ, S, J, and J_z.

If the nuclear short-range interaction is considered, the scattering wave function is still given by Eq. (11), but the coordinate wave function takes now the form

$$\Psi_{\ell S}^{JJ_z} = \sum_{\lambda S'} \frac{u_{\ell S}^{\lambda S'}(k, r)}{kr} \mathcal{Y}_{\lambda S'}^{JJ_z}(\hat{r}), \tag{12}$$

where we assume that, given an incoming channel with orbital angular momentum and spin $\{\ell, S\}$, the short-range interaction can mix it with an outgoing channel with quantum numbers $\{\lambda, S'\}$.

The general large distance behavior of the radial equations in Eq. (12) is given by

$$u_\ell^\lambda \to \delta_{\lambda\ell} F_\ell(\eta, kr) + T_{\lambda\ell} \mathcal{O}_\ell(\eta, kr), \tag{13}$$

where for simplicity we have assumed that the potential is diagonal in the spin, $u_\ell^\lambda \equiv u_{\ell S}^{\lambda S}$, and $\mathcal{O}_\ell(\eta, kr) = G_\ell(\eta, kr) + iF_\ell(\eta, kr)$ describes the outgoing wave function. In the expression above $T_{\lambda\ell}$ denotes the T-matrix elements which, in the case of a single channel, reduce to the usual form, $\sin\delta_\ell e^{i\delta_\ell}$, where δ_ℓ is the phase shift.

The antisymmetry requirement of the two-body wave function implies that $\{\ell, S\}$ and $\{\lambda, S\}$ become again $[\ell S]$ and $[\lambda S]$, which indicate that $S = 0$ ($S = 1$) for even (odd) values of ℓ and λ. Therefore, from Eqs. (11) and (12), and following the same procedure as in the free case, the norm of the wave

function results in

$$|\Psi_s|^2_\Omega = \frac{1}{2}\sum_{\lambda,\ell\equiv\text{even}}\left(\frac{u^\lambda_\ell(kr)}{kr}\right)^2(2\ell+1) + \frac{3}{2}\sum_{\lambda,\ell\equiv\text{odd}}\left(\frac{u^\lambda_\ell(kr)}{kr}\right)^2(2\ell+1), \quad (14)$$

which trivially reduces to Eq. (10) when the short-range interaction is absent.

B. Integration on a spherical source

To model the correlation function in Eq. (1) a parametrization of the source function is required. Starting from a single-particle emission source of a Gaussian form, the following two-body source function is obtained [Eq. (A4) in the Appendix]:

$$S_{12}(r) = \frac{1}{8\pi^{3/2}R^3}e^{-(r^2/4R^2)}, \quad (15)$$

where R is the source radius. The source function is normalized to unity in the coordinate space, and, therefore, it can be interpreted as the probability to emit particles at relative distance r.

The ALICE Collaboration developed a data-driven approach, called the resonance source model (RSM), able to describe the emission source in pp collisions at the LHC [34]. The RSM assumes the existence of a common emission source for all baryons, composed of a Gaussian core, from which all primordial particles are emitted, and an exponential tail caused by the strong decays of resonances into particles of interest. In Ref. [34], the core radius was determined from the fit of the measured pp correlation function as the pp interaction is already well constrained from scattering and nuclear data and the corresponding wave function can be precisely calculated for different energies. The pp correlation function was computed using the "Correlation Analysis Tool using the Schrödinger equation" (CATS) [35], which is a numerical framework capable of evaluating the correlation function by taking as input either an interaction potential or a two-particle wave function, as well as an emission source of any form. The Schrödinger equation was solved for the AV18 potential including s, p, and d waves, the Coulomb potential, and properly antisymmetrizing the pp wave function. The fit was performed for different transverse mass (m_T) ranges of the pairs and the scaling trend as a function of m_T, typically observed in heavy-ion experiments, was found. The transverse mass is defined as $m_T = (k_T^2 + m^2)^{1/2}$, where k_T and m are the average transverse momentum and the average mass of the pair, respectively. Further, in Ref. [34] it is demonstrated that with the proper inclusion of the strongly decaying resonances, the obtained Gaussian core radius in $p\Lambda$ measurements is, indeed, identical to the pp results, supporting the existence of a common emitting source for baryons in pp collisions.

The assumption of a common source for all the baryon-baryon pairs was used to test the interaction models of several hadron pairs and to access their low energy scattering properties through the correlation function. The source radius R for the hadron pairs of interest is determined from the m_T scaling, by using the average m_T of the measured pairs and considering the effective enlargement induced by the strong decaying resonances. In the case of pp pairs measured by the ALICE Collaboration, the effective m_T-integrated source radius amounts to $R = 1.249 \pm 0.008(\text{stat.})^{+0.024}_{-0.021}(\text{syst.})$ fm [9].

As shown in the Appendix, Eq. (A14), since the source is spherical, the correlation function can be computed as given in Eq. (1), but replacing $|\Psi_s|^2$ by $|\Psi_s|^2_\Omega$. After insertion of Eq. (10) the angular integration can be trivially performed, and we obtain that for particles interacting only through the Coulomb force the correlation function is given by

$$C^0_{12}(k) = \frac{1}{4\sqrt{\pi}R^3}\frac{1}{k^2}\int dr\, e^{-(r^2/4R^2)} \times\left(\sum_{\ell\equiv\text{even}}F^2_\ell(\eta,kr)(2\ell+1) + 3\sum_{\ell\equiv\text{odd}}F^2_\ell(\eta,kr)(2\ell+1)\right). \quad (16)$$

As an example, let us consider now the specific case in which the short-range interaction is limited to act on the $\ell = 0$ singlet state. In this case the norm, Eq. (14), can be written as

$$|\Psi_s|^2_\Omega = \left|\Psi^0_s\right|^2_\Omega + \frac{1}{2}\left[\left(\frac{u_0(kr)}{(kr)}\right)^2 - \left(\frac{F_0(\eta,kr)}{(kr)}\right)^2\right], \quad (17)$$

where we have added and subtracted the $\ell = 0$ free case contribution. The correlation function results in

$$C_{12}(k) = C^0_s + C_{00} = \int d\boldsymbol{r}\, S_{12}(r)\left[\left|\Psi^0_s\right|^2_\Omega - \frac{1}{2}\left(\frac{F_0(\eta,kr)}{kr}\right)^2 + \frac{1}{2}\left(\frac{u_0(kr)}{kr}\right)^2\right]. \quad (18)$$

The first term, C^0_s, is the component of the correlation function calculated with the free wave function without including the $\ell = 0$ contribution (the first two terms of the integral in the equation above), whereas the second term, C_{00}, is the $\ell = 0$ component including the interaction. Both terms are shown in Fig. 2 (top panel) using a source radius $R = 1.249$ fm together with the correlation function, $C^0_{12}(k)$, considering only the Coulomb force. The $\ell = 0$ radial wave function, $u_0(r)$, has been calculated using a Gaussian potential constructed to reproduce, in association with the Coulomb interaction, the pp scattering length and effective range. Specifically

$$V_{pp}(r) = V_0 e^{-(r/r_0)^2}\mathcal{P}_0 + \frac{e^2}{r} \quad (19)$$

with $V_0 = -30.45$ MeV and $r_0 = 1.815$ fm, $\mathcal{P}_0$ is a projector on spin $S = 0$. In fact, the s wave is well suited for a low-energy representation of the nucleon-nucleon (NN) potential by a two-parameter function, as the Gaussian used here, due to the dominance of the large value of the scattering length. This introduces the two-nucleon system inside the

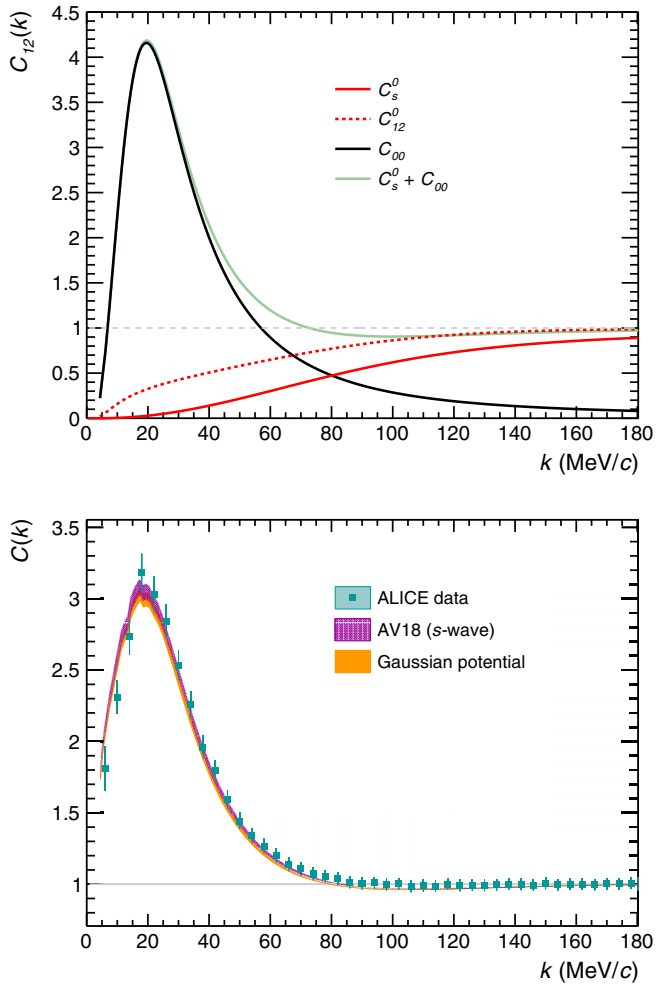

FIG. 2. *Top panel:* The *pp* correlation function calculated using a Gaussian potential acting in the singlet $\ell = 0$ channel. The source radius has been fixed to $R = 1.249$ fm. The $\ell = 0$ contribution is given by the black curve, the contribution of the other (free) partial waves is given by the red curve while the total result is given by the green curve. The correlation function considering only the Coulomb force is given by the red dashed curve. *Bottom panel:* The *pp* correlation function measured by the ALICE Collaboration (cyan data points) compared to the calculations obtained using the AV18 potential, considering only *s* wave (magenta band) and the prediction obtained using the Gaussian potential (orange band). The width of the bands represents the uncertainty due to the experimental determination of the source radius. The theoretical curves have been corrected to account for the experimental effects (see the text for the details).

universal window [18] in which universal behavior can be observed. A Gaussian representation of the NN interaction has been used many times in recent studies of the two-, three-, and four-nucleon systems [16,17,36,37], and even of nuclear matter [38]. The AV18 has been considered too, showing that essentially the two interactions give extremely close results for the *s*-wave component of the correlation function.

C. Comparison with the experimental data

In this section, the computed *pp* correlation function is compared to the experimental measurement published by the ALICE Collaboration [9]. The experimental correlation function is shown in Fig. 2 (bottom panel) with the cyan data points. The error bars include the combined contribution from the statistical and systematic uncertainties of the experiment, added in quadrature.

The experimental correlation function is obtained in terms of the particle momentum distributions (the formal derivation is shown in Ref. [1])

$$C(\boldsymbol{p}_1, \boldsymbol{p}_2) \equiv \frac{P(\boldsymbol{p}_1, \boldsymbol{p}_2)}{P(\boldsymbol{p}_1) \cdot P(\boldsymbol{p}_2)}, \tag{20}$$

where $P(\boldsymbol{p}_1, \boldsymbol{p}_2)$ is the two-particle momentum distribution, $P(\boldsymbol{p}_1)$ and $P(\boldsymbol{p}_2)$ are the single-particle momentum distributions. In absence of momentum correlations $P(\boldsymbol{p}_1, \boldsymbol{p}_2) = P(\boldsymbol{p}_1) \cdot P(\boldsymbol{p}_2)$, leading to $C(\boldsymbol{p}_1, \boldsymbol{p}_2) = 1$.

After removal of the two-body center-of-mass motion, Eq. (20) becomes

$$C(k) = \mathcal{N} \frac{A(k)}{B(k)}, \tag{21}$$

where $k = |\boldsymbol{p}_1 - \boldsymbol{p}_2|/2$ is the relative momentum between the two protons, $A(k)$ and $B(k)$ are the relative momentum distribution of correlated and uncorrelated protons, respectively, and $\mathcal{N}$ is a normalization constant. In the experimental analyses, $B(k)$ is obtained by pairing particles emitted in different collisions, using the so-called event mixing technique [3]. The obtained mixed event distribution needs to be then properly normalized to $A(k)$ in a k range where the interaction is absent. This normalization is absorbed in the factor $\mathcal{N}$. Following the arguments in Refs. [1,33], the correlation function in Eq. (21) can be related to the source and wave functions via the Koonin-Pratt formula introduced in Eq. (1).

To compare the experimental and the theoretical correlation functions, the latter has to be corrected for the following experimental effects: (1) momentum resolution of the detector which results in a smearing of the correlation function at low relative momenta; (2) the presence of secondary and misidentified protons in the experimental data sample. In the measurement performed by the ALICE Collaboration, the fraction of correctly identified primary protons amounts to $\lambda_{pp} = 0.67$, secondary protons are mainly produced in the decay of the Λ hyperons, corresponding to a fraction $\lambda_{pp_\Lambda} = 0.203$, while the other secondary and misidentification contributions amount to $\lambda_{\mathrm{X}} = 0.127$ [9]. The pairs with misidentified or secondary particles contribute to the measured correlation function as follows

$$C(k) = \lambda_{pp} C_{pp}(k) + \lambda_{pp_\Lambda} C_{pp_\Lambda}(k) + \lambda_{\mathrm{X}} C_{\mathrm{X}}(k). \tag{22}$$

The genuine *pp* correlation function $C_{pp}(k)$ is obtained from the theoretical correlation function $C_{12}(k)$ shown in Fig. 2, top panel, further corrected for the momentum resolution of the detector. As shown in Eq. (22), the comparison with the experimental correlation function requires an additional scaling by the factor λ_{pp}. The contribution $C_{pp_\Lambda}(k)$ results from the pairing of primary protons with those emitted in the decay of

a primary Λ particle, carrying the effect of the primary $p\Lambda$ interaction. The $p\Lambda$ correlation function has been modeled using chiral effective field theory calculations at the next-to-leading order (NLO) [39] and transformed into the relative momentum of the pp pairs by applying the corresponding decay matrices [9]. Following Ref. [9], all the remaining contributions to the measured correlation function are assumed to be flat, i.e., $C_X(k) = 1$.

The correlation function represented with a orange (magenta) band in the bottom panel of Fig. 2 is the resulting correlation function obtained from Eq. (22), by assuming the Gaussian (AV18) potential for the pp s-wave interaction described in the previous section to calculate $C_{pp}(k)$. The widths of the bands accounts for the experimental uncertainty on the source radius given in Ref. [9]. In this reference the pp correlation function was calculated using the AV18 interaction in s, p, and d waves, showing that the effects of the $\ell > 0$ partial waves are appreciable for $k > 100$ MeV/c, very far from the peak at 20 MeV/c. The agreement of the calculations with the ALICE data provides the benchmark of the procedure that will be extended to the three-body sector in the next section.

IV. THE THREE-BODY CASE

Three-body wave functions are usually described by means of the Jacobi coordinates $\boldsymbol{x}$ and $\boldsymbol{y}$, which for three identical particles read $\boldsymbol{x} = \boldsymbol{r}_2 - \boldsymbol{r}_1$ and $\boldsymbol{y} = \sqrt{4/3}\ [\boldsymbol{r}_3 - (\boldsymbol{r}_1 + \boldsymbol{r}_2)/2]$, where $\boldsymbol{r}_i$ is the position vector of particle i.

From these coordinates it is common to construct the hyperspherical coordinates, which contain one radial coordinate, the hyperradius $\rho = (x^2 + y^2)^{1/2}$, and five hyperangles [the four angles describing the direction of $\boldsymbol{x}$ and $\boldsymbol{y}$ plus $\alpha = \arctan(x/y)$] that we collect into Ω_ρ. From the $\boldsymbol{x}$ and $\boldsymbol{y}$ conjugate momenta, $\boldsymbol{k}_x$ and $\boldsymbol{k}_y$, we can also construct the hypermomentum $Q = (k_x^2 + k_y^2)^{1/2}$ and the five hyperangles Ω_Q equivalent to Ω_ρ, but in momentum space.

These coordinates are the ones employed in the hyperspherical harmonic (HH) formalism (see Ref. [40] and references therein). Within this method the three-body scattering wave function can be written as described in detail in the Appendix of Ref. [41], and which takes the form

$$\Psi_s = \frac{(2\pi)^3}{(Q\rho)^{5/2}} \sum_{JJ_z} \sum_{K\gamma} \Psi_{K\gamma}^{JJ_z} \sum_{M_L M_S} (LM_L SM_S|JJ_z) \mathcal{Y}_{KLM_L}^{\ell_x \ell_y}(\Omega_Q)^*, \tag{23}$$

where γ groups the quantum numbers $\{\ell_x, \ell_y, L, s_x, S\}$. Then ℓ_x and ℓ_y are the relative orbital angular momenta associated to the Jacobi coordinates $\boldsymbol{x}$ and $\boldsymbol{y}$, which couple to the total orbital angular momentum L (with projection M_L). The spin s_x denotes the total spin of the two nucleons connected by the $\boldsymbol{x}$ coordinate, which couples to the spin of the third nucleon to give the total three-body spin S (with projection M_S). The angular momenta L and S then couple to the total angular momentum of the system J with projection J_z. Finally, $K = 2\nu + \ell_x + \ell_y$ (with $\nu = 0, 1, 2, \ldots$) is the grand-angular momentum quantum number, and $\mathcal{Y}_{KLM_L}^{\ell_x \ell_y}$ are the usual hyperspherical harmonic functions.

Equation (23) is the three-body partner of Eq. (11). In fact, the coordinate wave functions, $\Psi_{K\gamma}^{JJ_z}$, take the general form

$$\Psi_{K\gamma}^{JJ_z} = \sum_{K'\gamma'} \Psi_{K\gamma}^{K'\gamma'}(Q, \rho) \Upsilon_{JJ_z}^{K'\gamma'}(\Omega_\rho), \tag{24}$$

with

$$\Upsilon_{JJ_z}^{K\gamma}(\Omega_\rho) = \sum_{M_L M_S} (LM_L SM_S|JJ_z) \mathcal{Y}_{KLM_L}^{\ell_x \ell_y}(\Omega_\rho) \chi_{SM_S}^{s_x}, \tag{25}$$

which are the three-body equivalents of Eqs. (12) and (4), respectively. As in Eq. (12), the radial wave function, $\Psi_{K\gamma}^{K'\gamma'}$, corresponds to a process with incoming and outgoing channels characterized by the set of quantum numbers $\{K, \gamma\}$ and $\{K', \gamma'\}$, respectively.

Following Eq. (6), we define again the norm of the scattering wave function as the average over the angular coordinates of the square of the wave function, i.e.,

$$|\Psi_s|_\Omega^2 = \frac{1}{\pi^6} \int d\Omega_\rho \int d\Omega_Q |\Psi_s|^2. \tag{26}$$

The three-body wave function as defined above does not have a well-defined symmetry under particle exchange. In order to introduce the correct symmetry we proceed as in the two-body case, and consider in Eq. (25) only the HH functions that, coupled to the spin functions, provide the correct total symmetry.

If the spin of the three-nucleon system is $S = \frac{1}{2}$, we have that Eq. (25) is given by

$$\Upsilon_{JJ_z}^{K\gamma}\left(S = \frac{1}{2}\right) = \sum_{M_L M_S} \left(LM_L \frac{1}{2} M_S|JJ_z\right) \sum_{\lambda} (-1)^\lambda \frac{\mathcal{Y}_{KLM_L}^{\ell_x \ell_y, \bar{\lambda}}(\Omega_\rho) \chi_{\frac{1}{2}M_S}^{\lambda}}{\sqrt{2}}, \tag{27}$$

where we have introduced the HH functions $\mathcal{Y}_{KLM_L}^{\ell_x \ell_y, \bar{\lambda}}$ having well defined values of angular momentum LM_L and mixed spin symmetry of type λ coupled to the spin $S = \frac{1}{2}$ of three nucleons defined as

$$\chi_{SS_z}^{\lambda} = \sum_{\sigma_x \sigma_y} \left(\lambda \sigma_x \frac{1}{2} \sigma_y|SS_z\right) \chi_{\lambda\sigma_x} \chi_{\frac{1}{2}\sigma_y}, \tag{28}$$

where $\chi_{\lambda\sigma_x}$ and $\chi_{\frac{1}{2}\sigma_y}$ are, respectively, the spin functions of the two-body system formed by the nucleons 1 and 2, and the one of the third nucleon. The quantum number $\lambda = 1, 0$ corresponds to the mixed spin symmetry, symmetric or antisymmetric with respect to the exchange of particles 1,2, respectively. With $\bar{\lambda}$ we indicate the conjugate symmetry, $\bar{\lambda} = 1$ when $\lambda = 0$ and vice versa.

In the case of $S = \frac{3}{2}$, since the spin part is always symmetric under exchange of nucleons 1 and 2, we have that

$$\Upsilon_{JJ_z}^{K\gamma}\left(S = \frac{3}{2}\right) = \sum_{M_L M_S} \left(LM_L \frac{3}{2} M_S|JJ_z\right) \mathcal{Y}_{KLM_L}^{\ell_x \ell_y, a}(\Omega_\rho) \chi_{\frac{3}{2}M_S}^{\frac{1}{2}}, \tag{29}$$

where we have introduced the antisymmetric HH functions, $\mathcal{Y}^{\ell_x\ell_y,a}_{KLM_L}$, coupled to the symmetric spin $S=\frac{3}{2}$ of three nucleons. Note that in both cases, $S=\frac{1}{2}$ and $\frac{3}{2}$, the index γ no longer includes the value of the spin of the two nucleons, s_x, since it is fixed by the symmetry requirements. This is similar to the two-body case, where the value of s_x is determined by the odd or even value of ℓ_x.

A. The case of three free neutrons

For the case of three free neutrons, since the Coulomb potential is absent, we have that [15]

$$\Psi^{K'\gamma'}_{K\gamma}(Q,\rho)=i^K\sqrt{Q\rho}J_{K+2}(Q\rho)\delta_{KK'}\delta\gamma\gamma', \tag{30}$$

where $J_{K+2}(Q\rho)$ is the Bessel function of order $K+2$, and the continuum wave function (23) simply becomes

$$\Psi^0_s=e^{i\boldsymbol{Q}\cdot\boldsymbol{\rho}}\sum_{SM_ss_x}\chi^{s_x}_{SM_S}. \tag{31}$$

Here the partial wave expansion of the three-body plane wave is given by

$$\begin{aligned}e^{i\boldsymbol{Q}\cdot\boldsymbol{\rho}}&=e^{i(\boldsymbol{k}_x\cdot\boldsymbol{x}+\boldsymbol{k}_y\cdot\boldsymbol{y})}\\&=\frac{(2\pi)^3}{(Q\rho)^2}\sum_{K\ell_x\ell_yLM_L}i^KJ_{K+2}(Q\rho)\mathcal{Y}^{\ell_x\ell_y}_{KLM_L}(\Omega_\rho)\mathcal{Y}^{\ell_x\ell_y}_{KLM_L}(\Omega_Q)^*.\end{aligned} \tag{32}$$

Using this partial wave expansion, we can verify that the norm of the three-body plane wave, Eq. (26), is given by

$$\frac{16}{3(Q\rho)^4}\sum_K J^2_{K+2}(Q\rho)(K+3)(K+2)^2(K+1)=1, \tag{33}$$

where we have used the following property of the HH functions:

$$\sum_{\ell_x\ell_yLM_L}\mathcal{Y}^{\ell_x\ell_y*}_{KLM_L}\mathcal{Y}^{\ell_x\ell_y}_{KLM_L}=\frac{1}{12\pi^3}(K+3)(K+2)^2(K+1). \tag{34}$$

Insertion of Eq. (31) into Eq. (26) leads to the same result for the norm of the free scattering function as in Eq. (7), i.e., $|\Psi^0_s|^2_\Omega=N_S$, but where now $N_S=8$ (four spin states from $S=\frac{3}{2}$, two from $S=\frac{1}{2}$ with $\lambda=0$, and two from $S=\frac{1}{2}$ with $\lambda=1$).

Considering antisymmetrization, we obtain that the norm of the free three-neutron scattering state, Eq. (26), becomes

$$\left|\Psi^0_s\right|^2_\Omega=\frac{6}{N_S}\frac{2^6}{(Q\rho)^4}\sum_K J^2_{K+2}(Q\rho)N_{ST}(K), \tag{35}$$

where, again, the factor of 6 (= 3!) enters due to the fact that we are dealing with three identical particles, the factor $1/N_S$ is introduced in order to impose $|\Psi^0_s|^2_\Omega\to 1$ as $Q\rho\to\infty$, and where $N_{ST}(K)$ is the number of states, depending on the grand angular quantum number K.

To calculate $N_{ST}(K)$ we have to consider that for each value of the grand angular quantum number, K, the HH functions can be symmetric, mixed, or antisymmetric. For the three-nucleon system in isospin $T=3/2$, only the last two can contribute to the wave function since the spin vector could be either of mixed symmetry ($S=\frac{1}{2}$) or symmetric ($S=\frac{3}{2}$). There is no antisymmetric spin state of three nucleons. The two mixed symmetry spin states having $S=\frac{1}{2}$ and $\lambda=0,1$ combine with two mixed HH functions, resulting in an antisymmetric state, whereas the symmetric spin state with $S=\frac{3}{2}$ is combined with the HH antisymmetric functions. Therefore the norm is

$$\left|\Psi^0_s\right|^2_\Omega=\frac{6}{N_S}\frac{2^6}{(Q\rho)^4}\sum_{K\geqslant 1}J^2_{K+2}(Q\rho)\left[N^m_{ST}(K)+4N^a_{ST}(K)\right] \tag{36}$$

with $N^m_{ST}(K)$ the number of mixed HH functions and $N^a_{ST}(K)$ the number of antisymmetric HH functions for each value of K. The factor 4 in front of $N^a_{ST}(K)$ is the spin degeneracy, whereas the spin degeneracy of 2 in the case of the mixed symmetry cancels out with the factor in the two-term sum as given in Eq. (27). The fact that the spatially symmetric state is not present implies that the sum starts with $K=1$.

The following algorithm can be used to determine the number of HH functions having different symmetries. The number of HH functions for a given K is [see Eq. (34)]

$$N=\frac{(K+1)(K+2)^2(K+3)}{12}. \tag{37}$$

The resulting ratio $r_n=N/N^m_{ST}$ is

$$r_n=\begin{cases}\frac{3}{2}\frac{(n_3-1)(n_3+1)}{n_3^2+3}, & n_3-2=K,\\ \frac{1}{2}\frac{(n_3+1)(n_3+2)}{n_3(n+1)}, & n_3-2\neq K,\end{cases} \tag{38}$$

where we have introduced the integer n defined as the integer part of $(K+2)/3$ and $n_3=3n$. Therefore $N^m_{ST}=N/r_n$. The number of antisymmetric HH functions is

$$N^a_{ST}=\begin{cases}\frac{N-N^m_{ST}}{2}, & K\text{ odd},\\ \frac{N-N^m_{ST}-m}{2}, & K\text{ even},\end{cases} \tag{39}$$

with $m=\frac{K}{2}+1$.

With the above considerations, the result from Eq. (36) is shown in Fig. 3. As seen in the figure, the norm tends to zero as $x\to 0$, since the sum starts at $K=1$, and goes asymptotically to 1.

B. Integration on a spherical source

In the case of three particles, the source function, analogous to Eq.(15), can be modeled as

$$S_{123}(\rho)=\frac{1}{\pi^3\rho_0^6}e^{-(\rho/\rho_0)^2}, \tag{40}$$

with the normalization condition

$$\int S_{123}(\rho)\rho^5 d\rho\, d\Omega_\rho=1. \tag{41}$$

The parameter ρ_0 of the three-particle source function is related to R_M, the parameter of the two-body source function, i.e., $\rho_0=2R_M$. This relation is discussed in the Appendix. The value of R_M must be determined experimentally from the m_T distribution of proton pairs emitted in *ppp* triplets. For this reason, we used a different notation with respect to the

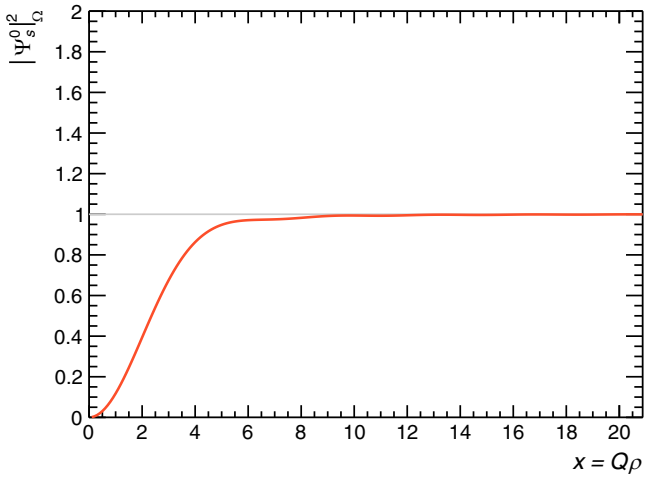

FIG. 3. Norm of the free scattering wave function for three neutrons, Eq. (36).

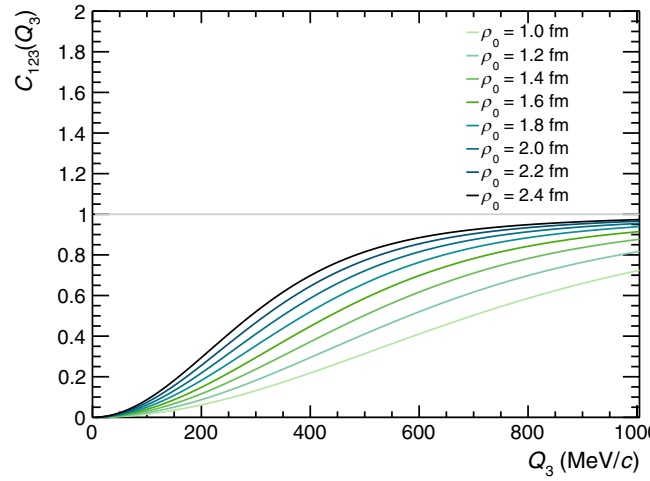

FIG. 4. The correlation function using the free scattering wave function for three neutrons, Eq. (42), calculated using different source sizes.

radius R introduced in Sec. II B. In general, the average m_T of two protons which are emitted in pairs or triplets could be different in the experimental data sample and, additionally, the properties of the source function for three particles has not been studied yet. Recently, a numerical framework capable of simulating the effective emission source of a n-body system, based on the properties of the single particles, was developed [42], but it has not been tested yet to the data due to the limitations in terms of statistics of the Run 2 ALICE data. This will be possible thanks to the larger statistics that has being acquired during the ongoing LHC Run 3 data campaign. By approximating $R_M \simeq R = 1.249$ fm, which is the value used to model the pp correlation function, we find $\rho_0 \simeq 2.5$ fm. For the reasons mentioned above, this value of ρ_0 is not anchored to any realistic three-body source model and, therefore, a scan over different values of ρ_0 will be done in the next sections.

The three-body correlation function is defined in Eq. (2). As in the two-body case (see the Appendix), due to the spherical symmetry of the source function, we can replace $|\Psi_s|^2$, given in Eq. (23), by $|\Psi_s|^2_\Omega$, given in Eq. (26). In the particular case of free nnn, making use of Eq. (35) with $N_S = 8$, we trivially get from the definition in Eq. (2) that

$$C_{123}(Q) = \frac{6}{8}\frac{2^6}{Q^4\rho_0^6}\int \rho\, d\rho\, e^{-\frac{\rho^2}{\rho_0^2}} \sum_K J^2_{K+2}(Q\rho) N_{ST}(K). \tag{42}$$

In Fig. 4 we can see the correlation function C_{123} calculated using different source sizes. Note that Q refers to the total energy $E = \hbar^2 Q^2/2m$ whereas the three-body momentum Q_3, used in some figures, is defined in Sec. V C. It verifies $Q_3 = \sqrt{6}Q$ and is the experimentally detected quantity.

C. Introducing the interaction

The analytical form of the three-body continuum wave function given in Eqs. (23) and (24) is completely general. As shown in Eq. (30), for three noninteracting nucleons, the matrix formed by the radial wave functions, $\Psi^{K'\gamma'}_{K\gamma}$, is diagonal. However, when a short-range particle-particle interaction is present, this matrix is in general nondiagonal, in such a way that the incoming and outgoing channels, characterized by quantum numbers $\{K, \gamma\}$ and $\{K', \gamma'\}$, respectively, can be different.

When using the HH formalism, one of the difficulties is that the basis set used in the wave function expansion in Eq. (24) can be quite large, which leads to a large system of coupled radial equations from which the matrix of radial wave functions can be obtained.

On many occasions, it is convenient to employ a different basis set, that we denote as $\Phi^{JJ_z}_n(\rho, \Omega_\rho)$, where n labels the different terms of the basis, depending not only on the hyperangles, Ω_ρ, but also on the hyperradius, ρ. The transformation between this basis set and the one in Eq. (25) is given by

$$\Phi^{JJ_z}_n(\rho, \Omega_\rho) = \sum_{K\gamma} \left\langle \Upsilon^{K\gamma}_{JJ_z}(\Omega_\rho) \middle| \Phi^{JJ_z}_n(\rho, \Omega_\rho) \right\rangle_{\Omega_\rho} \Upsilon^{K\gamma}_{JJ_z}(\Omega_\rho), \tag{43}$$

where the functions $\Upsilon^{K\gamma}_{JJ_z}(\Omega_\rho)$ are given in Eq. (25), $\langle\,|\,\rangle_\Omega$ represents integration over the angular coordinates, and the summation over the HH quantum numbers K and $\gamma \equiv \{\ell_x \ell_y L S\}$ has to be truncated at some maximum values $K_{\max}$ and $\gamma_{\max}$.

Using the new basis set, the three-body continuum wave function can be written as described in detail in Appendix D of Ref. [15], and takes the form

$$\Psi_s = \frac{(2\pi)^3}{(Q\rho)^{5/2}} \sum_{JJ_z} \sum_n u^J_n \sum_{s_x S M_S} \left\langle \chi^{s_x}_{SM_S} \middle| \Phi^{JJ_z}_n(Q, \Omega_Q) \right\rangle^*, \tag{44}$$

where

$$u^J_n = \sum_{n'} u^{n'}_n(Q, \rho) \Phi^{JJ_z}_{n'}(\rho, \Omega_\rho), \tag{45}$$

and the incoming and outgoing channels are now n and n', respectively.

Equations (44) and (45) are equivalent to Eqs. (23) and (24) in the HH formalism. In fact, the latter are recovered from Eqs. (44) and (45) simply by using that [15]

$$u_n^{n'}(Q,\rho) = \sum_{K'\gamma'}\sum_{K\ell_x\ell_y L} \Psi_{K\gamma}^{K'\gamma'}(Q,\rho)\langle \Phi_{n'}^{JJ_z}(\rho,\Omega_\rho)|\Upsilon_{JJ_z}^{K'\gamma'} \times (\Omega_\rho)\rangle_{\Omega_\rho}\langle \Upsilon_{JJ_z}^{K\gamma}(\Omega_Q)|\Phi_n^{JJ_z}(Q,\Omega_Q)\rangle_{\Omega_Q}, \quad (46)$$

and recalling that $\sum_n |\Phi_n\rangle\langle\Phi_n| = \mathbb{1}$.

In this work, we shall use the hyperspherical adiabatic (HA) expansion method, described in detail in Ref. [12], where the $\{\Phi_n\}$ basis set is chosen to be formed by the eigenfunctions of the angular part of the Hamiltonian equation,

$$H_\Omega \Phi_n^{JJ_z}(\rho,\Omega_\rho) = U_n(\rho)\Phi_n^{JJ_z}(\rho,\Omega_\rho), \quad (47)$$

in such a way that the eigenvalue functions, $U_n(\rho)$, enter as effective potentials in a coupled set of radial equations from which the $u_n^{n'}$ radial functions are obtained (see [12] for details).

One of the main advantages of the HA method is that most of the dynamics of the system is captured by the lowest terms in the adiabatic expansion in Eq. (44). As a consequence, very few terms in the expansion, typically around ten, are enough for an accurate description of the continuum wave function [15,43]. This reduces drastically the number of radial equations to be computed, and therefore the size of the matrix formed by the radial wave functions, $u_n^{n'}$.

The reason for such a convenient behavior of the HA expansion can be understood by noting that, when only short-range interactions are involved (as in the *nnn* case), each adiabatic potential $U_n(\rho)$ in Eq. (47) behaves asymptotically as $K(K+4)/\rho^2$. In such a way, each term of the HA basis tends to a single HH basis element term:

$$\Phi_n^{JJ_z}(\rho,\Omega) \to \Upsilon_{JJ_z}^{K\gamma}(\Omega). \quad (48)$$

This permits one to associate a specific grand-angular momentum value, K, to each adiabatic channel n. In fact, the asymptotic behavior of the continuum $u_n^{n'}(Q,\rho)$ functions takes the form

$$u_n^{n'}(Q,\rho\to\infty) \to i^{K'}\sqrt{Q\rho}[\delta_{KK'}J_{K'+2}(Q\rho) + T_{KK'}\mathcal{O}_{K'+2}(Q\rho)], \quad (49)$$

where K and K' are the grand-angular momentum values associated with the incoming and outgoing channels n and n', respectively, $\mathcal{O}_{K+2}(Q\rho) = Y_{K+2}(Q\rho) + iJ_{K+2}(Q\rho)$ is the outgoing asymptotic wave function, $T_{KK'}$ is a T-matrix element, and $J_{K+2}(Q\rho)$, $Y_{K+2}(Q\rho)$ are the regular and irregular Bessel functions.

It should be noticed that when inserting Eq. (49) into the expression of the full continuum wave function, Eq. (44), the second term, proportional to the T matrix, tends to zero as K increases, since the interaction that produces the coupling between the different HH channels remains hidden by the centrifugal barrier $K(K+4)/\rho^2$. On the other hand channels with increasing values of K are important as the energy increases.

Following Eqs. (35) and (49), the norm of the scattering wave function for the three-body state with total angular momentum J tends asymptotically to

$$|\Psi^J|^2_\Omega(\rho\to\infty) = (2J+1)\frac{6}{8}\frac{2^6}{(Q\rho)^5}\sum_{KK'}\left|u_K^{K'}(Q,\rho\to\infty)\right|^2 N_{ST}(K), \quad (50)$$

where $u_K^{K'}(Q,\rho\to\infty)$ is normalized as given in Eq. (49), and the $(2J+1)$ factors appears after summation over all the possible J_z projection quantum numbers. After summation over all the possible J states, the norm becomes

$$\sum_J |\Psi^J|^2_\Omega = \frac{6}{8}\frac{2^6}{(Q\rho)^4}\sum_J(2J+1) \times \left(\sum_{KK'}^{K_0}\left|\frac{u_K^{K'}(Q,\rho)}{\sqrt{Q\rho}}\right|^2 + \sum_{K>K_0} J_{K+2}^2(Q\rho)\right) N_{ST}(K), \quad (51)$$

where K_0 is the quantum number indicating the maximum value of K at which the interaction distorts the free scattering state. For $K > K_0$ the wave function is taken as the free solution; i.e., for $K > K_0$, $u_K^{K'}(Q,\rho)$ is replaced by $i^{K'}\sqrt{Q\rho}\delta_{KK'}J_{K'+2}(Q\rho)$.

D. The *nnn* correlation function

In order to calculate the three-neutron correlation function, we model the *nn* interaction with a Gaussian potential for the singlet channel, $S = 0$:

$$V_{nn}(r) = V_0 e^{-(r/r_0)^2}\mathcal{P}_0, \quad (52)$$

with the parameters $V_0 = -30.42$ MeV and $r_0 = 1.8148$ fm selected to reproduce the *nn* s-wave scattering length and effective range of -18.9 ± 0.4 fm and 2.8 ± 0.1 fm, respectively [44].

Since the spatially symmetric state is not present in the *nnn* system, we have that the only states for which the lowest adiabatic HH channel (going asymptotically to $K = 1$) contributes are the $J^\pi = 1/2^-, 3/2^-$ states.

We first consider the $J^\pi = 1/2^-$ state with total angular momentum $L = 1$ ($\ell_x = 0$, $\ell_y = 1$) and total spin $S = 1/2$. If we consider the $K = 1$ adiabatic channel only, making use of Eqs. (45), (48), and (49) we get that the asymptotic form of Eq. (44) is given by

$$\Psi_{\rm HA}^{1/2^-} \overset{\rho\to\infty}{\longrightarrow} \frac{i(2\pi)^3}{(Q\rho)^2}[J_3(Q\rho) + T_{11}\mathcal{O}_3(Q\rho)]\Upsilon_{\frac{1}{2}^-}^{1\gamma_1}(\Omega_\rho)\langle\chi_{S=\frac{1}{2}}|\Upsilon_{\frac{1}{2}^-}^{1\gamma_1}(\Omega_Q)\rangle, \quad (53)$$

where $\gamma_1 \equiv \{\ell_x = 0, \ell_y = 1, L = 1, S = \frac{1}{2}\}$.

If we assume that the interaction distorts very little the behavior of the adiabatic channels for $n > 1$, the wave function of the $1/2^-$ state can be written as

$$\Psi^{1/2^-} = \Psi_{\rm HA}^{1/2^-} + \Psi_0^{1/2^-}, \tag{54}$$

where the free wave function is defined as

$$\Psi_0^{1/2^-} = \frac{(2\pi)^3}{(Q\rho)^2} \sum_{K\geqslant 3} i^K J_{K+2}(Q\rho) \Upsilon^{K\gamma_1}_{\frac{1}{2}^-}(\Omega_\rho) \left\langle \chi_{S=\frac{1}{2}} \middle| \Upsilon^{K\gamma_1}_{\frac{1}{2}^-}(\Omega_Q) \right\rangle. \tag{55}$$

Here the sum over K starts at $K = 3$ since the $K = 1$ asymptotic term is included in $\Psi_{\rm HA}^{1/2^-}$.

The norm of the wave function of Eq. (54) can be computed as given in Eq. (26), and it can be written as

$$\left|\Psi^{1/2^-}\right|^2_\Omega = \left|\Psi_{\rm HA}^{1/2^-}\right|^2_\Omega + \left|\Psi_0^{1/2^-}\right|^2_\Omega + \left\langle \Psi_{\rm HA}^{1/2^-} \middle| \Psi_0^{1/2^-} \right\rangle_\Omega + \left\langle \Psi_0^{1/2^-} \middle| \Psi_{\rm HA}^{1/2^-} \right\rangle_\Omega, \tag{56}$$

where the first two terms in the right-hand side are the norms of $\Psi_{\rm HA}^{1/2^-}$ and $\Psi_0^{1/2^-}$, respectively. The last two terms arise from the interference between the two wave functions, and, by use of Eqs. (44) and (55), one can easily get that

$$\left\langle \Psi_{\rm HA}^{1/2^-} \middle| \Psi_0^{1/2^-} \right\rangle_\Omega = \frac{(2\pi)^6}{(Q\rho)^5} \sum_{K>1}^{K_{\rm max}} w_1^K(\rho) J_{K+2}(Q\rho), \tag{57}$$

where $w_1^K(\rho) = \sqrt{Q\rho}\, u_1^1(\rho) \langle \Upsilon^{K\gamma}_{\frac{1}{2}^-} | \Phi_1^{\frac{1}{2}^-} \rangle_{\Omega_\rho}$.

The correlation function is then computed after inserting the expression given in Eq. (56) into Eq. (2). It can be seen that the contribution of the interference terms of Eq. (57) is very small, since the term $K = 1$ is not present and $w_K^1(\rho \to \infty) = 0$ for $K > 1$, whereas $J_{K+2}(Q\rho \to 0) = (Q\rho/2)^{K+2}/(K+2)!$. This is illustrated in Fig. 5, where the contribution to the correlation function arising from the $J^\pi = 1/2^-$ state is shown when one and two adiabatic channels are considered. The label "tail" indicates that free contributions are included for values of $K > 1$ or $K > 3$ in each of the two cases. As we can see, inclusion of the second adiabatic channel slightly modifies the computed curve only in the large momentum region. In fact, as seen in the inset of the figure (where a zoom of the curves is shown), the result with one adiabatic channel plus the tail basically overlaps with the result with two adiabatic channels (for which the inclusion of the tail makes no visible change). When the square of the wave function is taken, Eq. (56), the interference terms are automatically included. However, in the inset of the figure we can also see that removal of the interference contributions hardly modifies the computed curve. The conclusion is that one adiabatic channel is sufficient to treat the interaction, whereas higher channels can be considered as free.

In Fig. 6 the correlation function including the $J^\pi = 1/2^-$ and $J^\pi = 3/2^-$ states with $\rho_0 = 2$ fm is analyzed. The convergence in terms of $K_{\rm max}$, the maximum grand-angular momentum quantum number used to describe the adiabatic potentials, is very fast; a value of $K_{\rm max} = 31$ is already sufficiently accurate. Moreover the lowest adiabatic component, $n = 1$, gives the main contribution to the correlation function.

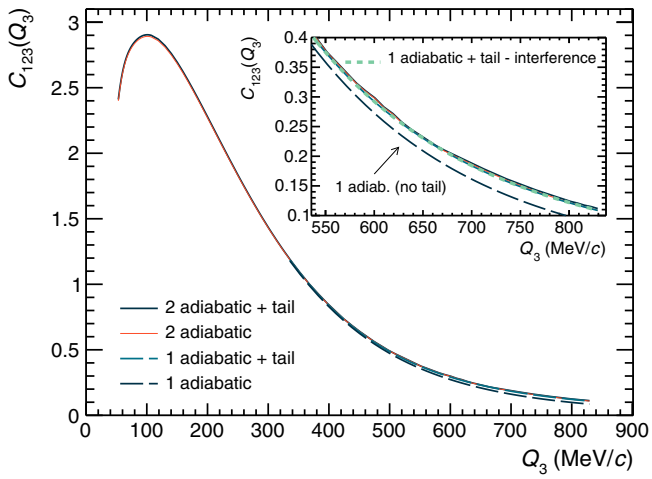

FIG. 5. The $J^\pi = 1/2^-$ contributions to the correlation function. One or two adiabatic channels are considered with and without the inclusion of higher contributions treated as free (tail).

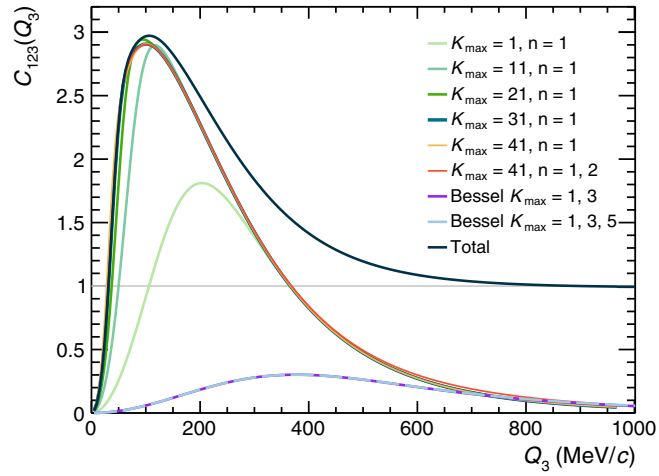

FIG. 6. The contribution to the correlation function of the states $J^\pi = 1/2^-, 3/2^-$ for three neutrons computed with one ($n = 1$) or two ($n = 2$) adiabatic channels calculated up to the indicated value of $K_{\rm max}$. The curves indicated by "Bessel" use Bessel functions as hyperradial functions in the indicated channels (see text). The total curve (black) is the correlation function computed using one adiabatic channel for the states $J^\pi = 1/2^-, 3/2^-$, calculated using HH functions up to $K_{\rm max} = 31$, with the other states starting at $K = 2$ considered free.

In fact, in the figure the contribution of the second component, $n = 2$, is shown, and it almost overlaps with the results given just using only one adiabatic component. The curves labeled by "Bessel $K_{\max} = 1, 3$" and "Bessel $K_{\max} = 1, 3, 5$" are calculated using the Bessel functions as hyperradial function and, as can be seen, they overlap above 200 MeV with the curves in which the interaction has been considered. This indicates that for high values of Q_3 the correlation function can be calculated using the free form. The total curve includes the effects of the interaction in the lowest two adiabatic channels with the rest of the contribution coming from the other channels considered as free, as given in Eq. (51).

V. THE CASE OF THREE PROTONS: INCLUDING THE COULOMB FORCE

The Coulomb force for a system of three protons is

$$V_{\rm Coul} = \sum_{i<j} \frac{e^2}{r_{ij}}, \tag{58}$$

where r_{ij} is the distance between particles i and j. Implementation of this interaction in a three-body calculation has the significant complication that the matrix formed by the matrix elements of this potential between different basis terms (either within the HH or the HA methods) is not diagonal, even asymptotically. Furthermore, the asymptotic behavior of the continuum wave functions is not known analytically, and this makes it rather difficult to extract the T matrix that enters, for instance, in Eq. (53).

We postpone a complete treatment of the Coulomb interaction to a forthcoming work, and explore here the influence of the Coulomb force in the correlation function as an average of the force on the hyperangles, i.e.,

$$V_{\rm Coul}(\rho) = \frac{1}{\pi^3} \int d\Omega_\rho \sum_{i<j} \frac{e^2}{r_{ij}} = \frac{3(4\pi)^2}{\pi^3} \int d\alpha \sin^2\alpha \cos^2\alpha \frac{e^2}{\rho \cos\alpha} = \frac{16}{\pi} \frac{e^2}{\rho}, \tag{59}$$

which transforms the Coulomb potential into a function depending only on the hyperradius ρ. The above equation can be considered as a 0-term in an expansion of the Coulomb potential in terms of HH multipoles (K expansion). It should be noticed that a symmetric $K = 2$ HH function does not exist, and, therefore, the next term of the expansion will be the 4-term. This property makes operative the hypercentral approximation of the Coulomb in the calculation of the *ppp* correlation function (for a more complete treatment of the Coulomb interaction see Refs. [45,46]).

When solving the three-body problem, the hypercentral Coulomb potential enters directly as a potential in the set of coupled equations providing the hyperradial wave functions. Disregarding for the moment the nuclear force, the radial equations for each value of the grand-angular momentum K are given by

$$\left(\frac{\partial^2}{\partial z^2} + 1 - \frac{2\eta}{z} - \frac{(K+\frac{3}{2})(K+\frac{5}{2})}{z^2} \right) u_K(z) = 0, \tag{60}$$

with $z = Q\rho$ and $\eta = 16me^2/(\pi\hbar^2 Q)$, where m is the proton mass.

When $\eta \neq 0$ (*ppp* case), the solution of the equation above is

$$u_K(z) = F_{K+\frac{3}{2}}(\eta, z), \tag{61}$$

which is the regular Coulomb function with order $K + \frac{3}{2}$ and Sommerfeld parameter η, and which for $\eta = 0$ (*nnn* case) reduces to

$$u_K(z) = z j_{K+\frac{3}{2}}(z) = \sqrt{\frac{\pi z}{2}} J_{K+2}(z). \tag{62}$$

Therefore, for the free *ppp* system, the norm of the continuum wave function is the same as in the *nnn* case, Eq. (35), but with the replacement

$$J_{K+2}(z) \longrightarrow \sqrt{\frac{2}{\pi z}} F_{K+\frac{3}{2}}(z). \tag{63}$$

When this is done, we get

$$|\Psi_s^0|^2_\Omega = \frac{96}{\pi} \frac{1}{(Q\rho)^5} \sum_K F^2_{K+3/2}(Q\rho) N_{ST}(K). \tag{64}$$

As in the *nnn* case, if the antisymmetrization of the three protons is not taken into account, the number of states is given in Eq. (37), whereas in the case of antisymmetrization it is

$$N_{ST}(K) = N^m_{ST}(K) + 4N^a_{ST}(K). \tag{65}$$

The results for the norm given in Eq. (64) are shown in Fig. 7. Note that the curve obtained implementing antisymmetrization, but without the Coulomb interaction, coincides with the one of Fig. 3.

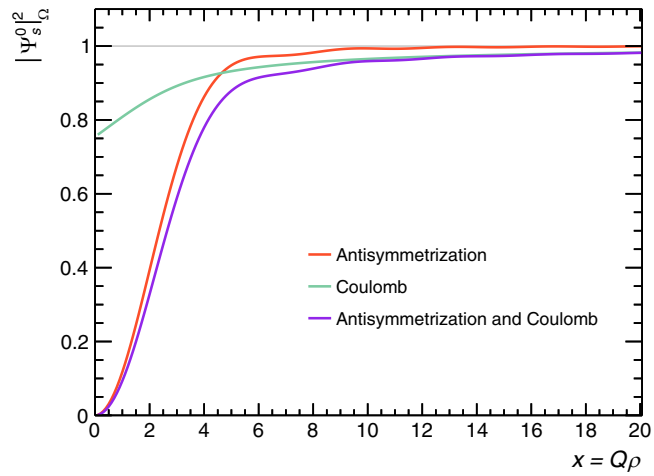

FIG. 7. The norm of the free scattering wave function for three protons with and without considering the hypercentral Coulomb force and antisymmetrization.

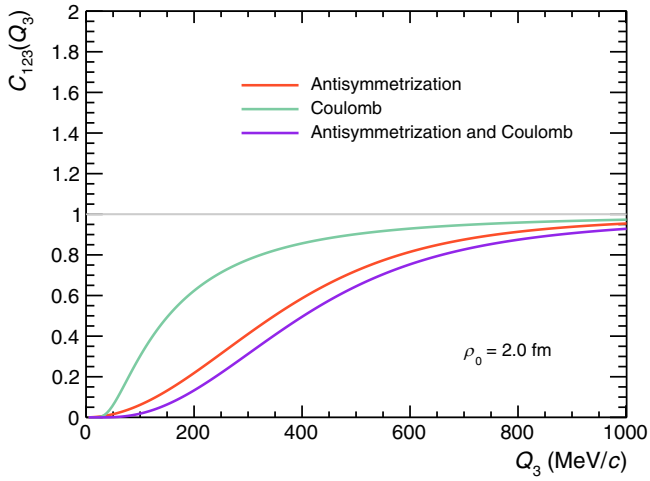

FIG. 8. Same as Fig. 7 but for the correlation function.

A. Integrating on a spherical source

The free *ppp* correlation function obtained after integrating on a spherical source, Eq. (2), coincides with the one of the *nnn* system, Eq. (42), with the substitution indicated in Eq. (63). We therefore obtain

$$C_{123}(Q) = \frac{96}{\pi}\frac{1}{Q^5\rho_0^6}\int d\rho\, e^{-\frac{\rho^2}{\rho_0^2}} \sum_K F^2_{K+3/2}(Q\rho) N_{ST}(K). \tag{66}$$

In Fig. 8 we show $C_{123}(Q_3)$ obtained using $\rho_0 = 2$ fm, and we compare the no Coulomb case (red curve) with the Coulomb case (violet curve). The green curve shows the case in which no antisymmetrization of the three protons is taken into account.

B. Introducing the interaction

The procedure used to introduce the interaction among the three protons is the same as described for the *nnn* system. We therefore use the HA expansion method, and the only difference is that the numerical solutions for the radial functions, $u_n^{n'}$, in Eq.(45), are obtained including the hypercentral potential of Eq. (59).

The consequence is that the asymptotic behavior of the $u_n^{n'}(Q,\rho)$ functions is now

$$u_n^{n'}(Q,\rho\to\infty) \to i^{K'}\sqrt{\frac{2}{\pi}}\left[\delta_{KK'}F_{K'+\frac{3}{2}}(\eta,Q\rho) + T_{KK'}\mathcal{O}_{K'+\frac{3}{2}}(\eta,Q\rho)\right], \tag{67}$$

which is simply the same as for the *nnn* system, Eq. (49), but, once more, with the substitution of Eq. (63), which applies as well for the irregular functions, in such a way that $\mathcal{O}_K(\eta,Q\rho) = iF_K(\eta,Q\rho) + G_K(\eta,Q\rho)$.

With the same procedure adopted for the *nnn* case, we obtain, in analogy with Eq. (51), that the norm of the scattering wave function for the *ppp* systems is given by

$$\sum_J |\Psi^J|^2_\Omega = \frac{96}{\pi}\frac{1}{(Q\rho)^5}\sum_J(2J+1) \times\left(\sum_{KK'}^{K_0}\left|\frac{u_K^{K'}(Q,\rho)}{\sqrt{2/\pi}}\right|^2 + \sum_{K>K_0}F^2_{K+\frac{3}{2}}(\eta,Q\rho)\right)N_{ST}(K), \tag{68}$$

where, again, K_0 is the quantum number indicating the maximum value of K at which the interaction distorts the free scattering state. Note that the factor $\sqrt{2/\pi}$ that divides the $u_K^{K'}(Q,\rho)$ function is a consequence of the normalization given in Eq. (67), and permits recovering the regular Coulomb function in the free case.

As a first application of the formalism to the *ppp* case we consider two different models for the *pp* interaction. First, as in the two-body case, we model the short-range *pp* interaction with a Gaussian potential in spin $S = 0$ [see Eq. (19)], with the parameters selected to reproduce the *pp* scattering length and effective range of -7.8063 ± 0.0026 fm and 2.773 ± 0.014 fm, respectively [44]. In addition we consider also the AV18 NN interaction.

As in the *nnn* system, we use the HA method and solve the hyperradial equations for the lowest adiabatic channel. The only two states having asymptotically the lowest HH channel ($K = 1$) compatible with parity and antisymmetrization are the $J^\pi = 1/2^-$ and $3/2^-$ states. In the same way, the lowest adiabatic channel with $K = 2$ is consistent with the $J^\pi = 1/2^+$, $3/2^+$, and $5/2^+$ states. For the Gaussian interaction, the adiabatic channels calculated with the values $K_{\max} = 31$ ($K_{\max} = 30$) odd (even) parity states are sufficient to get convergence in the corresponding adiabatic channels. However when using the AV18 interaction much higher values are considered, $K_{\max} = 151$ ($K_{\max} = 150$) for odd (even) parity states. After solving the adiabatic equations to obtain the hyperradial functions $u_K^{K'}(Q,\rho)$, the norm of the scattering *ppp* wave function is completely determined. The states with $J^\pi = 1/2^-, 3/2^-$ and $J^\pi = 1/2^+, 3/2^+, 5/2^+$ are given by the first term of Eq. (68) with $K_0 = 2$, whereas the second term includes all the other channels. Making use of the norm, and integrating over ρ as given in Eq. (2), we obtain the *ppp* correlation function for each of the cases.

We first study the impact of $K_{\max}$ on the correlation function. In Fig. 9 this is shown for the two potential models and using a source size value of $\rho_0 = 2$ fm. As mentioned, the interaction has been included in the $J^\pi = 1/2^-, 3/2^-$ states and $J^\pi = 1/2^+, 3/2^+, 5/2^+$ states with $K_0 = 1$ and $K_0 = 2$, respectively. The free scattering wave function has been considered for $K > 2$. In other words, the figure shows the correlation function obtained using Eq. (68) with $K_0 = 2$ and, for the AV18 potential, at different values of $K_{\max}$ in the computation of the hyperradial functions $u_K^{K'}(Q,\rho)$. It is interesting to observe that the converged results for the Gaussian and the AV18 potential are on top of each other in the very low Q region. However the values of $K_{\max}$ needed to

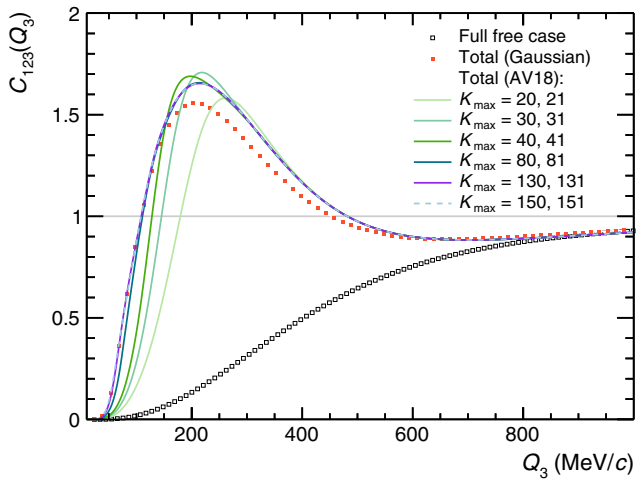

FIG. 9. The *ppp* correlation function with a source size of $\rho_0 = 2$ fm, calculated using the first adiabatic channel for asymptotic states with $K = 1, 2$, considering different values of $K_{\max}$. For $K > 2$ the free scattering function is considered. The full free case is also shown.

reach convergence are very different. In fact, as can be seen in the figure, the AV18 curves for $K_{\max} \geqslant 130$ almost overlap. Moreover, we can observe a higher peak when this potential is used. This is due to contributions beyond the pure s wave at which the Gaussian potential is limited. We also see that with increasing Q the effect of the short-range interaction smears out and the correlation function is well described by the free scattering wave function.

We now study different partial wave contributions to the *ppp* correlation function. This is shown in Fig. 10 where the different J^π contributions are shown explicitly for the two potential models. The results were computed using a source size of 2.0 fm. We observe that the use of the realistic force

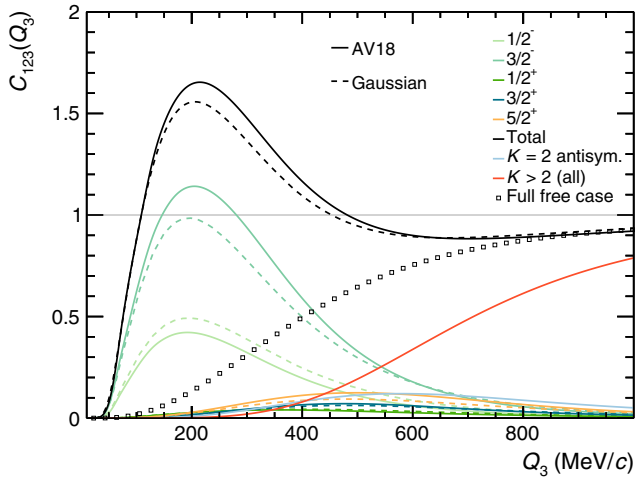

FIG. 10. The *ppp* correlation function using the AV18 potential (solid lines) and comparison to the results using a Gaussian interaction (dashed lines). The source size $\rho_0 = 2.0$ fm was used. The Coulomb free contribution is also shown.

slightly increases the observable value around the peak, which is mainly due to the contribution of the $J^\pi = 3/2^-$ state. As is evident from the figure, the peak of the observable is almost completely constructed by the odd-parity components of the wave function. This means that detailed measurements of the *ppp* correlation function around the peak could be used to asses the capability of the potential models to produce the correct splitting of the three-body P waves' phase shifts, a problem already observed in the description of asymmetries as the *pd* A_y analyzing power (for a recent discussion see Ref. [47]).

To complete the study of the correlation function, we also performed calculations using the AV18 potential plus the Urbana IX three-body force. We observed differences, in the direction of reducing the correlation function, of the order of 1% or lower. This confirms the very small effect of the three-body force in the *ppp* and *nnn* systems already observed in Ref. [16] for the latter. This is mainly due to the Pauli principle which prevents the three equal nucleons from being close enough to feel the influence of the three-nucleon force.

Finally we discuss the effects of the source size. In the top panel of Fig. 11, we show, as a function of the hyperradius, the overlap of the source function, $\pi^3\rho^5 S_{123}(\rho)$, with the short-range potential averaged on the hyperangles, i.e., defined as

$$V(\rho) = \frac{1}{\pi^3}\int d\Omega_\rho \sum_{i<j} V_0(r_{ij}). \tag{69}$$

For this purpose we have used the s-wave part of the AV18 potential. As can be seen from the figure, the effect of the potential is more appreciable for source sizes larger than 2 fm. In the bottom panel, the correlation function is shown for the different source radii. Moreover, the correlation function considering only the Coulomb potential is explicitly shown as dashed lines.

C. Comparison with the experimental data

In this section, the calculated *ppp* correlation function is compared to the experimental one published by the ALICE Collaboration in Ref. [5]. The experimental correlation function is shown in Fig. 12 as cyan squares.[1] The vertical lines correspond to the statistical uncertainties while the boxes denote systematic ones. The measured three-body correlation function is obtained in a similar way as explained for the two-body case in Sec. III C. However, Eq. (21) is extended to three particles as

$$C(Q_3) = \mathcal{N}\frac{A(Q_3)}{B(Q_3)}. \tag{70}$$

Here, $A(Q_3)$ corresponds to the same event triplets, while the distribution $B(Q_3)$ is obtained by combining three particles from three different events. The observable Q_3 is Lorentz invariant and is estimated experimentally as $Q_3 = \sqrt{-q_{12}^2 - q_{23}^2 - q_{31}^2}$, where q_{ij} is the norm of the four-vector

[1]The first bin, published by the ALICE Collaboration, is not shown here; however, it is at a correlation function value of 3.5.

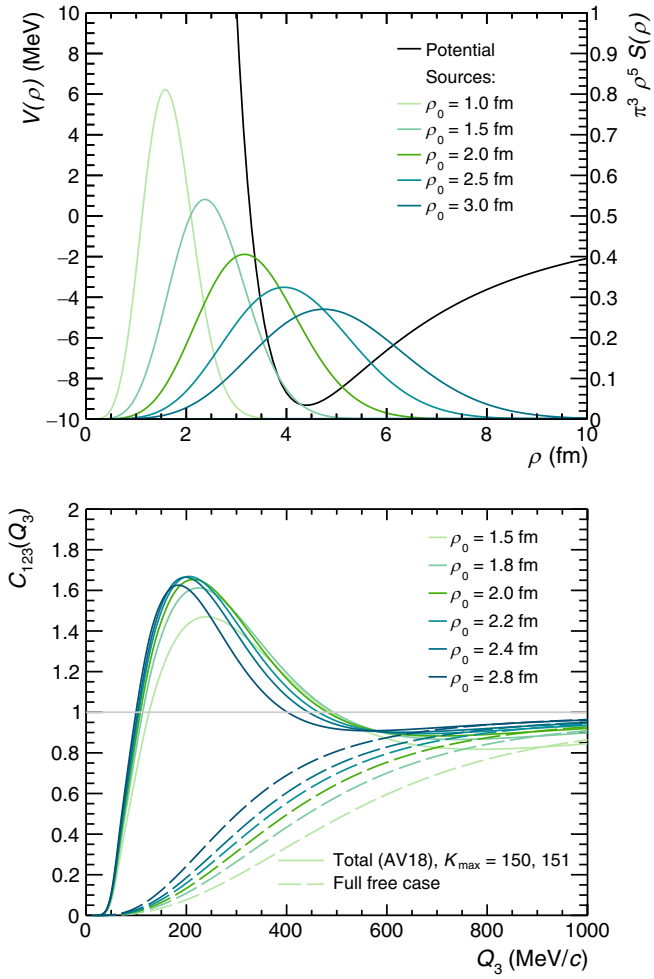

FIG. 11. *Top panel:* Overlap between the average s-wave potential and the source function for different radii. *Bottom panel:* The ppp correlation function calculated using the AV18 potential for different source radii (solid lines). The Coulomb free contributions are shown with dashed lines.

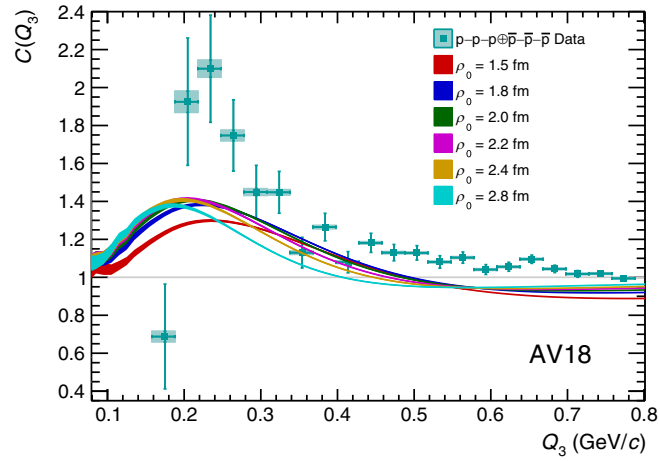

FIG. 12. The comparison of the ppp correlation function measured by the ALICE Collaboration [5] (cyan full squares) and the calculated correlation functions corrected for experimental effects (bands). The vertical lines on the data points correspond to the statistical uncertainties and the boxes to the systematic ones. Different color bands correspond to the different source sizes. For details of corrected correlation functions, refer to the text.

corresponding to the relative momentum between particles i and j [5]. The normalization constant $\mathcal{N}$ is such that the measured correlation function is equal to unity at Q_3 region, where particles are expected to not interact anymore via final state interaction [5].

As has been explained previously, the calculated correlation functions cannot be compared directly to the measured ones since the experimental effects such as momentum resolution and the presence of secondary and misidentified protons must be taken into account. The momentum resolution can be included by performing a convolution of the theoretical correlation function, the mixed event distribution, and the momentum resolution matrix as described in Ref. [24]. This was done by employing the mixed event distribution and momentum resolution matrix recently published by the ALICE Collaboration in Ref. [48]. The effect of secondary and misidentified protons can be taken into account by employing Eq. (22) extended to the three-particle case as

$$C(Q_3) = \lambda_{ppp} C_{ppp}(Q_3) + \lambda_{ppp_\Lambda} C_{ppp_\Lambda}(Q_3) + \lambda_X C_X(Q_3). \tag{71}$$

$C_{ppp}(Q_3)$ is here included as the calculated correlation function shown in Fig. 11 with the fraction of genuine ppp triplets being $\lambda_{ppp} = 0.618$ [5]. The residual $pp\Lambda$ correlation function $C_{ppp_\Lambda}(Q_3)$, where one of the protons is a product of Λ decay, is obtained by taking the $C_{pp\Lambda}(Q_3)$ correlation function and performing a convolution with the decay matrix which maps the Q_3 of initial $pp\Lambda$ triplet to the Q_3 of the resulting ppp triplet after the Λ decay. The $pp\Lambda$ correlation function is known only experimentally and has been measured by the ALICE Collaboration [5]. However, the published values are provided only up to $Q_3 = 0.8$ GeV/c. When used to estimate the $C_{ppp_\Lambda}(Q_3)$ correlation function, this results in edge effects at the range $Q_3 > 0.55$ GeV/c. For this reason, the $pp\Lambda$ correlation function at values larger than $Q_3 = 0.8$ GeV/c is assumed to be equal to the projector values published in Ref. [5], which are shown to be in good agreement with data. The fraction of $pp\Lambda$ triplets in the experimental sample is $\lambda_{pp\Lambda} = 0.196$ [5]. In Eq. (71), the $\lambda_X C_X(Q_3)$ term includes the rest of the contributions, such as protons stemming from other hyperon decays or misidentified proton contribution. The correlation functions for $C_{ppH}(Q_3)$, where H denotes hyperons other than Λ which decay to protons, are not known. However, the λ parameters for single channels are very small and thus, after accounting for the decay kinematics, $C_{ppp_H}(Q_3)$ are expected to be equal to unity. The correlation function for misidentified protons is also assumed to be equal to unity. Thus $C_X(Q_3)$ in Eq. (71) is also assumed to be equal to unity. The resulting correlation functions $C(Q_3)$ are shown in Fig. 12 as colorful bands for different source sizes, already accounting

for momentum resolution effects. The bands include propagated systematic and statistical uncertainties of $C_{pp\Lambda}(Q_3)$.

The comparison in Fig. 12 shows that the calculated correlation functions are systematically below the experimental data in the entire range $Q_3 < 0.8$ GeV/c, independently of the chosen value for the source size ρ_0. In contrast, the shape is well reproduced. The experimental correlation function obtained in Ref. [5] was normalized to unity in the range $1.0 < Q_3 < 1.2$ GeV/c, assuming that any effect induced by the final state interaction of the three protons is absent in such an interval. This argument was motivated by the analysis of the pp pair correlations in ppp triplets and Monte Carlo studies (see Ref. [5] for more details). Interestingly, the calculation performed in this paper evidences the presence of residual correlations also at large Q_3. These correlations result in a dominantly repulsive effect at $Q_3 > 0.5$ GeV/c mainly due to the antisymmetrization of the ppp wave function. A proper comparison between the data and the theory would require extending the experimental measurements to a larger Q_3 interval, including the region where the theoretical correlation function converges to unity. Note that this study has to be considered preliminary, as further improvements in the modeling are required concerning, in particular, the source function.

VI. CONCLUSIONS

In the present work we have made a detailed analysis of the *nnn* and *ppp* correlation functions. This study was motivated by the recent effort to measure the *ppp* correlation function from high-energy pp collisions at the LHC. The main difficulties in the computation of this observable arise from the complicated structure of the asymptotic *ppp* wave function induced by the long range Coulomb interaction and the different spatial-spin structures needed to fulfill the Pauli principle requirements. In this analysis we performed a simplification and treated the Coulomb interaction using the hypercentral approximation. This approximation is well motivated by the absence of the $K = 2$ term in the expansion of the Coulomb interaction in terms of HH functions. Accordingly we can solve the associate dynamical equations with boundary conditions similarly to the *nnn* case. To this end we made use of HA method, showing that the lowest adiabatic potential already gives an extremely accurate description of the dynamics. In a first step we used a simple potential model consisting in a Gaussian interaction parametrized in order to reproduce the pp scattering length and effective range. This simplified interaction captures most of the structure of the observable in both, the two-body and the three-body sectors. This is mainly motivated by the large value of pp scattering length when the Coulomb interaction is switched off. Motivated by the encouraging results in the description of the *ppp* correlation function using the mentioned approximations, in a second step we considered the AV18 interaction. The main modification with the precedent results was found in the $3/2^-$ state with a higher peak and, consequently an overall increase of the observable. Note that the inclusion of the Urbana IX three-body force, very important in the description of nuclei, gives a negligible contribution in the correlation function mainly due to the low probability of having three protons close to each other.

The present results complete the study of the three-nucleon correlation function initiated with the study of the pd correlation function [6,7]. It shows that the measurements of these observables from high energy collisions open the door to a new way of studying reactions in different three-body systems. In particular it would be possible to use the present method, the HH basis in conjunction with the HA expansion, to describe the $pp\Lambda$ correlation function already measured by the ALICE Collaboration.

ACKNOWLEDGMENTS

The authors gratefully acknowledge Laura Fabbietti for the fruitful discussions that helped the improvement of the paper. This work was partially supported by Grant No. PID2022-136992NB-I00 funded by MCIN/AEI/10.13039/501100011033; by "ERDF A way of making Europe" from the European Union and the "European Union NextGenerationEU/PRTR"; by the Deutsche Forschungsgemeinschaft through Grant No. SFB 1258 "Neutrinos and Dark Matter in Astro- and Particle Physics"; and by the Deutsche Forschungsgemeinschaft (DFG, German Research Foundation) under Germany's Excellence Strategy, EXC 2094 390783311.

APPENDIX: THE SOURCE FOR TWO AND THREE PARTICLES

The correlation function of a pair of (identical) particles can be written in general as (here, for simplicity, we disregard the particle spins)

$$C_{12}(\boldsymbol{p}_1, \boldsymbol{p}_2) = \int d^3r_1\, d^3r_2 S_1(r_1) S_1(r_2) \times |\Psi(\boldsymbol{p}_1, \boldsymbol{p}_2, \boldsymbol{r}_1, \boldsymbol{r}_2)|^2, \tag{A1}$$

where $\Psi(\boldsymbol{p}_1, \boldsymbol{p}_2, \boldsymbol{r}_1, \boldsymbol{r}_2)$ denotes the two-particle scattering wave function that asymptotically describes particle 1 (2) with momentum $\boldsymbol{p}_1$ ($\boldsymbol{p}_2$). In Eq. (A1) $S_1(r)$ describes the spatial shape of the source for single-particle emissions. It can be approximated as a Gaussian probability distribution with a width R_M, which is defined as follows:

$$S_1(r) = \frac{1}{\left(2\pi R_M^2\right)^{\frac{3}{2}}} e^{-r^2/2R_M^2}. \tag{A2}$$

R_M is also known as the source size for single particle emission. Equation (A1) can be simplified by noting that in the wave functions the dependence on the overall center-of-mass (CM) coordinate can be trivially factored out. Introducing the CM coordinate $\boldsymbol{R}_{\rm CM} \equiv \frac{\boldsymbol{r}_1+\boldsymbol{r}_2}{2}$ and the relative distance $\boldsymbol{r} \equiv \boldsymbol{r}_1 - \boldsymbol{r}_2$, and rewriting the two-particle wave function as $\Psi(\boldsymbol{p}_1, \boldsymbol{p}_2, \boldsymbol{r}_1, \boldsymbol{r}_2) = e^{-i\boldsymbol{R}_{\rm CM}\cdot\boldsymbol{P}}\psi_{\boldsymbol{k}}(\boldsymbol{r})$, lead to the Koonin-Pratt relation for two-particle correlation function [32,33], which we write here as

$$C_{12}(k) = \int d^3r\, S(r)|\psi_{\boldsymbol{k}}(\boldsymbol{r})|^2, \tag{A3}$$

where $\psi_{\boldsymbol{k}}(\boldsymbol{r})$ represents the two-particle relative wave function, with $\boldsymbol{k} = (\boldsymbol{p}_1 - \boldsymbol{p}_2)/2$, and $S(r)$ is the two-particle emission source, given by

$$S(r) = \left(\frac{1}{4\pi R_M^2}\right)^{3/2} e^{-\frac{r^2}{4R_M^2}}. \tag{A4}$$

This source is identical to that given in Eq. (15), so we can identify R with the single-particle source radius R_M.

The generalization to the calculation of the correlation function of three identical particles is given by

$$C_{123}(Q) = \int d^3r_1 d^3r_2 d^3r_3 \; S_1(r_1) S_1(r_2) S_1(r_3) |\Psi_s|^2, \tag{A5}$$

where Q and Ψ_s were defined at the beginning of Section IV. Since we are considering the case of three identical particles, for all of them the source is assumed to have the same form as that given in Eq. (A2).

Equation (A5) can be simplified by introducing the following variables:

$$\boldsymbol{x} = \boldsymbol{r}_2 - \boldsymbol{r}_2, \quad \boldsymbol{y}' = \boldsymbol{r}_3 - \frac{\boldsymbol{r}_1 + \boldsymbol{r}_2}{2}, \quad \boldsymbol{R}_3 = \frac{1}{3}(\boldsymbol{r}_1 + \boldsymbol{r}_2 + \boldsymbol{r}_3). \tag{A6}$$

Now

$$d^3r_1 d^3r_2 d^3r_3 = d^3R_3 d^3x d^3y' \tag{A7}$$

and

$$S_1(r_1) S_1(r_2) S_1(r_3) = \frac{e^{-(3R_3^2 + \frac{2}{3}y'^2 + \frac{1}{2}x^2)/2R_M^2}}{\left(2\pi R_M^2\right)^{\frac{9}{2}}}. \tag{A8}$$

Integrating over d^3R_3 (the wave function Ψ_s does not depend on R_3), we obtain

$$C_{123}(Q) = \int d^3x d^3y' \; \frac{e^{-(\frac{4}{3}y'^2 + x^2)/4R_M^2}}{\left(3\pi R_M^2\right)^{\frac{3}{2}} \left(4\pi R_M^2\right)^{\frac{3}{2}}} |\Psi_s|^2. \tag{A9}$$

In term of the Jacobi vector $\boldsymbol{y} = \sqrt{\frac{4}{3}}\boldsymbol{y}'$ (see the beginning of Sec. IV), this integral can be rewritten as

$$C_{123}(Q) = \left(\frac{3}{4}\right)^{\frac{3}{2}} \int d^3x \, d^3y \times \frac{e^{-(x^2+y^2)/4R_M^2}}{\left(3\pi R_M^2\right)^{\frac{3}{2}} \left(4\pi R_M^2\right)^{\frac{3}{2}}} |\Psi_s|^2 . \tag{A10}$$

Introducing the hyperradius (see again the beginning of Sec, IV), given by $\rho = \sqrt{x^2 + y^2}$, and the hyperangular variables Ω_ρ [10], such that $d^3x \, d^3y = \rho^5 d\rho \, d\Omega_\rho$, we finally obtain

$$C_{123}(Q) = \int \rho^5 d\rho d\Omega_\rho \; S_{123}(\rho) |\Psi_s|^2, \tag{A11}$$

where

$$S_{123}(\rho) = \frac{e^{-\rho^2/4R_M^2}}{(4\pi R_M^2)^3}, \tag{A12}$$

and which after comparison with Eqs. (2) and (40) permits us to identify $\rho_0 = 2R_M$ (see, however, the discussion at the end of Sec. V C).

Starting with a Gaussian shape for the single-particle emission, the result is that two- and three-particle emission sources are spherical. Accordingly, the correlation functions in Eqs. (1) and (2) can be obtained after replacing $|\Psi_s|^2$ by the "angle averaged" square modulus of the wave functions.

For example, in the experimental detection of two protons, all pairs with the same k but arbitrary direction Ω_k are counted to construct $C_{12}(k)$. This is equivalent to performing the average $\frac{1}{4\pi} \int d\Omega_k |\Psi_s|^2$, and the correlation function in Eq. (1) can then be computed as

$$C_{12}(k) = \int r^2 dr \, d\Omega_r S_{12}(r) \left[\frac{1}{4\pi} \int d\Omega_k |\Psi_s|^2\right]. \tag{A13}$$

Since the source function is spherical, Eq. (A13) can be trivially rewritten as

$$C_{12}(k) = \int r^2 dr \, d\Omega'_r S_{12}(r) \left[\frac{1}{(4\pi)^2} \int d\Omega_r \int d\Omega_k |\Psi_s|^2\right], \tag{A14}$$

which makes clear that the correlation function $C_{12}(k)$ can be computed as given in Eq. (1), but replacing $|\Psi_s|^2$ by the "angle averaged" norm of the scattering wave function as defined in Eq. (6).

The same situation results in the three body case. The detection of three protons at a fixed value of Q is equivalent to performig the average over Ω_Q. Noting that $\int d\Omega_Q = \int d\Omega_\rho = \pi^3$, and following the same reasoning as shown above for the two-body case, we have that the correlation function $C_{123}(Q)$ can also be computed as given in Eq. (2), but replacing now $|\Psi_s|^2$ by the "angle averaged" norm of the scattering wave function given in Eq. (26).

[1] U. A. Wiedemann and U. W. Heinz, Phys. Rep. **319**, 145 (1999).

[2] U. Heinz and B. V. Jacak, Annu. Rev. Nucl. Part. Sci. **49**, 529 (1999).

[3] M. A. Lisa, S. Pratt, R. Soltz, and U. Wiedemann, Annu. Rev. Nucl. Part. Sci. **55**, 357 (2005).

[4] L. Fabbietti, V. Mantovani Sarti, and O. Vázquez Doce, Annu. Rev. Nucl. Part. Sci. **71**, 377 (2021).

[5] S. Acharya *et al.* (ALICE Collaboration), Eur. Phys. J. A **59**, 145 (2023).

[6] S. Acharya *et al.* (ALICE Collaboration), arXiv:2308.16120 [nucl-ex].

[7] M. Viviani, S. König, A. Kievsky, L. E. Marcucci, B. Singh, and O. Vázquez Doce, Phys. Rev. C **108**, 064002 (2023).

[8] S. L. Yakovlev, JETP Lett. **116**, 268 (2022).

[9] S. Acharya *et al.* (ALICE Collaboration), Phys. Lett. B **805**, 135419 (2020).

[10] A. Kievsky, S. Rosati, M. Viviani, L. E. Marcucci, and L. Girlanda, J. Phys. G **35**, 063101 (2008).

[11] L. E. Marcucci, J. Dohet-Eraly, L. Girlanda, A. Gnech, A. Kievsky, and M. Viviani, Front. Phys. **8**, 69 (2020).
[12] E. Nielsen, D. V. Fedorov, A. S. Jensen, and E. Garrido, Phys. Rep. **347**, 373 (2001).
[13] A. Kievsky, M. Viviani, and S. Rosati, Phys. Rev. C **64**, 024002 (2001).
[14] A. Kievsky, M. Viviani, and L. E. Marcucci, Phys. Rev. C **69**, 014002 (2004).
[15] E. Garrido, A. Kievsky, and M. Viviani, Phys. Rev. C **90**, 014607 (2014).
[16] M. D. Higgins, C. H. Greene, A. Kievsky, and M. Viviani, Phys. Rev. Lett. **125**, 052501 (2020).
[17] M. D. Higgins, C. H. Greene, A. Kievsky, and M. Viviani, Phys. Rev. C **103**, 024004 (2021).
[18] A. Kievsky, M. Gattobigio, L. Girlanda, and M. Viviani, Annu. Rev. Nucl. Part. Sci. **71**, 465 (2021).
[19] R. B. Wiringa, V. G. J. Stoks, and R. Schiavilla, Phys. Rev. C **51**, 38 (1995).
[20] B. S. Pudliner, V. R. Pandharipande, J. Carlson, and R. B. Wiringa, Phys. Rev. Lett. **74**, 4396 (1995).
[21] S. Acharya *et al.* (ALICE Collaboration), Phys. Rev. C **99**, 024001 (2019).
[22] S. Acharya *et al.* (ALICE Collaboration), Phys. Rev. Lett. **124**, 092301 (2020).
[23] S. Acharya *et al.* (ALICE Collaboration), Eur. Phys. J. C **83**, 340 (2023).
[24] S. Acharya *et al.* (ALICE Collaboration), Phys. Lett. B **833**, 137272 (2022).
[25] S. Acharya *et al.* (ALICE Collaboration), Phys. Lett. B **797**, 134822 (2019).
[26] S. Acharya *et al.* (ALICE Collaboration), Phys. Rev. Lett. **123**, 112002 (2019).
[27] S. Acharya *et al.* (ALICE Collaboration), Phys. Lett. B **845**, 138145 (2023).
[28] S. Acharya *et al.* (ALICE Collaboration), Nature (London) **588**, 232 (2020).
[29] S. Acharya *et al.* (ALICE Collaboration), Phys. Lett. B **844**, 137223 (2023).
[30] S. Acharya *et al.* (ALICE Collaboration), Phys. Rev. Lett. **127**, 172301 (2021).
[31] S. Acharya *et al.* (ALICE Collaboration), Phys. Lett. B **829**, 137060 (2022).
[32] S. E. Koonin, Phys. Lett. B **70**, 43 (1977).
[33] S. Pratt, T. Csorgo, and J. Zimanyi, Phys. Rev. C **42**, 2646 (1990).
[34] S. Acharya *et al.* (ALICE Collaboration), Phys. Lett. B **811**, 135849 (2020).
[35] D. L. Mihaylov *et al.*, Eur. Phys. J. C **78**, 394 (2018).
[36] A. Tumino, G. G. Rapisarda, M. La Cognata *et al.*, Commun. Phys. **6**, 106 (2023)
[37] M. Gattobigio, A. Kievsky, and M. Viviani, Phys. Rev. C **100**, 034004 (2019).
[38] A. Kievsky, M. Viviani, D. Logoteta, I. Bombaci, and L. Girlanda, Phys. Rev. Lett. **121**, 072701 (2018).
[39] J. Haidenbauer, U. G. Meißner, and A. Nogga, Eur. Phys. J. A **56**, 91 (2020).
[40] M. Fabre de la Ripelle, Ann. Phys. (NY) **147**, 281 (1983)
[41] B. V. Danilin, T. Rogde, J. S. Vaagen, I. J. Thompson, and M. V. Zhukov, Phys. Rev. C **69**, 024609 (2004).
[42] D. Mihaylov and J. González González, Eur. Phys. J. C **83**, 590 (2023).
[43] E. Garrido, C. Romero-Redondo, A. Kievsky, and M. Viviani, Phys. Rev. A **86**, 052709 (2012).
[44] R. Machleidt and D. Entem, Phys. Rep. **503**, 1 (2011).
[45] A. Kievsky, E. Garrido, M. Viviani, and M. Gattobigio, arXiv:2402.06317 [nucl-th].
[46] E. Garrido, A. Kievsky, and M. Viviani, Few-Body Syst. **57**, 1227 (2016).
[47] L. Girlanda, E. Filandri, A. Kievsky, L. E. Marcucci, and M. Viviani, Phys. Rev. C **107**, L061001 (2023).
[48] ALICE Collaboration, CERN Report No. ALICE-PUBLIC-2023-006, 2023 (unpublished).